Global distribution of aerosol direct radiative forcing in the ultraviolet and visible arising under clear skies

By N. HATZIANASTASSIOU[1]*, B. KATSOULIS[2] and I. VARDAVAS[3],   [1]*Laboratory of Meteorology, Department of Physics, University of Ioannina, 45110 Ioannina, Greece, and Foundation for Research and Technology-Hellas, Heraklion, Crete, Greece;* [2]*Laboratory of Meteorology, Department of Physics, University of Ioannina, Ioannina, Greece;* [3]*Department of Physics, University of Crete, and Foundation for Research and Technology-Hellas, Heraklion, Crete, Greece*

ABSTRACT

A deterministic atmospheric spectral radiative transfer model, that uses comprehensive climatological data, is developed to compute the global distribution of mean monthly clear-sky total direct aerosol radiative forcing in the ultraviolet (UV) and visible, between 0.2–0.85 μm, at the top of the atmosphere (TOA), within the atmosphere and at the Earth's surface for winter and summer conditions. The aerosol data were taken from the Global Aerosol Data Set (GADS), given for various fixed relative humidity values and for 11 wavelengths within the UV–visible range, both for natural and anthropogenic aerosols. We first derive global climatologies of extinction aerosol optical thickness (AOT), single-scattering albedo (ω_{aer}) and asymmetry factor (g_{aer}), for actual relative humidity values within the aerosol layer, based on the National Centers for Environmental Prediction and National Center for Atmospheric Research (NCEP/NCAR) Reanalysis Project and the Tiros Operational Vertical Sounder (TOVS) datasets. We include the global distribution of cloud cover using the D2 data from the International Satellite Cloud Climatology Project (ISCCP), to define the clear-sky fraction at the pixel level for each month. Supplementary 10-yr climatological data for surface and atmospheric parameters were taken from NCEP/NCAR, ISCCP-D2 and TOVS. Our present analysis allows the aerosol radiative properties and forcings to vary with space, time and wavelength. The computed mean annual global AOT, ω_{aer} and g_{aer} values are found to be 0.08, 0.96 and 0.73, respectively, at 0.5 μm. On a mean monthly 2.5° pixel resolution, aerosols are found to decrease significantly the downward and the absorbed solar radiation at the surface, by up to 28 and 23 W m^{-2}, respectively, producing a surface cooling at all latitudes in both winter and summer. Aerosols are found to generally increase the outgoing solar radiation at TOA (planetary cooling) while they increase the solar atmospheric absorption (atmospheric warming). However, the model results indicate that significant planetary warming, by up to 5 W m^{-2}, can occur regionally, such as over desert areas, due to strong aerosol absorption. A smaller planetary warming (by up to 2 W m^{-2}) is also found over highly reflecting ice- or snow-covered areas, such as Antarctica and Greenland, as well as over Eastern Europe, Siberia and North America. In general, the aerosol-induced surface cooling exceeds the induced atmospheric warming, except for regions characterized by strong aerosol absorption (e.g. deserts). On a mean annual global basis, natural plus anthropogenic aerosols are found to cool the Earth by 0.6 W m^{-2} (they increase the planetary albedo by 0.28%), to heat the atmosphere by 0.8 W m^{-2}, while they decrease the downward and net surface solar radiation (surface cooling) by about 1.9 and 1.4 W m^{-2}.

1. Introduction

The suspended particulate matter in the atmosphere is very important in determining the Earth's climate in many aspects. Aerosols are involved in complex two-sided interactions with other atmospheric constituents, e.g. gases or clouds, as well as with climate, and they perturb the radiation field sufficiently to warrant their consideration in any discussion of processes that

maintain the current climate (IPCC, 2001). Inclusion of aerosols is now necessary in climatic change studies that examine changes in surface and atmospheric temperatures, snow- and ice-cover extent, sea-level rise, precipitation changes, frequency and intensity of extreme weather events, and desertification, since aerosols crucially affect the radiation budget at the top of the atmosphere (TOA), in the atmosphere and at the surface, and hence atmospheric dynamics as well as evaporation and surface energy balance. Besides, aerosols are considered to be probably responsible for the disagreement between model estimates and measurements of downward surface solar radiation. Aerosols affect

---

*Corresponding author.
e-mail: nhatzian@cc.uoi.gr

the Earth's radiation budget in two ways. First, they scatter and absorb solar radiation, and so they modify the planetary albedo and reduce the amount of radiation reaching the surface; this is known as the direct effect of aerosols (Charlson et al., 1991, 1992; IPCC 2001). Secondly, aerosols act as cloud condensation nuclei, thereby modifying the microphysical (e.g. droplet number), micro-chemical, and hence optical and radiative properties of clouds, e.g. albedo (first indirect effect, Twomey 1974; Jones et al., 1994; Schwartz, 1996; IPCC, 2001); besides, aerosols also decrease the cloud precipitation efficiency (second indirect effect, Charlson et al., 1992; IPCC, 2001). Both total effects act against, and are believed to partly offset, the long-wave (LW) forcing induced by increasing emissions of greenhouse gases (IPCC, 2001). However, the aerosol short-wave (SW) forcing behaves quite differently to the greenhouse LW forcing in several important ways (Charlson et al., 1992); a major difference is that aerosols have much shorter atmospheric lifetime (from 10^{-4} for natural to tens of days for anthropogenic aerosols) compared with the important greenhouse gases (decades to centuries). This, together with microphysical and mixing processes, results in larger spatial and temporal aerosol variability. Thus, quantification of direct aerosol SW forcing is more complex than quantification of radiative forcing by greenhouse gases (IPCC, 2001).

One way to solve the problem is to estimate the aerosol direct SW forcing by using climate models that are able to represent adequately the physical structure of the Earth's atmosphere including aerosols. Nevertheless, these models require comprehensive global microphysical, micro-chemical, optical and radiative aerosol properties. However, despite the progress that has been made, it is very difficult to define a global aerosol climatology. Field (surface and aircraft) measurements cannot provide a global aerosol climatology and all the aerosol properties required by models, although an extensive series of regional field campaigns have taken place recently (e.g. Tropospheric Aerosol Radiative Forcing Observational Experiment, TARFOX, Aerosol Characterization Experiment, ACE-1, ACE-2, Indian Ocean Experiment, INDOEX) while monitoring networks, such as the National Aeronautics and Space Administration (NASA) Aerosol Robotic Network (AERONET) provide essential information on the chemical and physical properties of aerosols. Characteristics such as size distribution, composition and optical properties, are critical to aerosol radiative forcing and have to be adequately determined on a global scale. Older aerosol databases, with limited data from a few monitoring networks did not meet this need. The situation improved in the 1990s, when large organizations (e.g. the World Meteorological Organization, WMO) were engaged in expanding the existing surface-based monitoring networks. In the meantime, technological and instrument development has offered new possibilities for measuring the aerosol properties. Space-based observing systems and remote sensing offer an alternative and they are promising, since they are naturally suited to global cover-

age. Recently, sophisticated instruments (e.g. Moderate Resolution Imaging Spectro-Radiometer, MODIS, and Polarization and Directionality of the Earth's Reflectance, POLDER) are helping to establish a satellite-based network (e.g. National Aeronautics Space Administration, NASA, Global Aerosol Climatology Project, GACP) to complement surface-based monitoring networks (e.g. AERONET). However, although significant progress has been made over the last 10 years, many difficulties still exist in retrieving AOT precisely, over land, and especially over high-albedo surfaces. Besides, no validated satellite climatology yet provides global distributions of the aerosol single-scattering albedo, which is difficult to retrieve, especially over oceans (Kaufman et al., 1997). There exist some Total Ozone Mapping Spectrometer (TOMS) ω_{aer} data, but for use in local studies. Furthermore, no global climatology provides data on the aerosol asymmetry factor, though it is also important in determining the aerosol direct effect and is required for modelling the solar radiative transfer through aerosols. Apart from satellite measurements, global aerosol models are at present valuable tools, and substantially help to provide a global picture of the amount of atmospheric aerosols, their major characteristics and temporal variations, as well as their physico-chemical, optical properties and their radiative effects, though there is a degree of uncertainty associated with their use.

Attempts to estimate the global direct radiative forcing of aerosols started in the 1970s (Kahle and Deirmendjan 1973; Joseph et al., 1976) and continued through the 1980s (e.g. Coakley and Cess, 1985), with rather large concentrations and simple estimates of the aerosol properties. Lately, a series of assessments of aerosol climatic effects has appeared. Many recent studies of the direct aerosol SW forcing have concentrated upon the distributions and radiative effects of anthropogenic scattering sulphate aerosols, which are believed to produce a substantial cooling effect (Langner, and Rodhe, 1991; Charlson et al., 1992; Kiehl and Briegleb, 1993; Taylor and Penner 1994; Roeckner et al., 1995; Boucher and Anderson, 1995; Feichter et al., 1997; Penner et al., 1998; Kiehl et al., 2000, among others). On the other hand, recent attention has been directed to mineral-dust aerosols, especially those originating from changes in land use, because of their large contribution to atmospheric aerosol loading and absorption of solar radiation (e.g. Li et al., 1996; Sokolik and Toon, 1996; Tegen et al., 1996). Recently, numerous studies have investigated the optical properties and radiative effects of a mixture of sulphate and carbonaceous aerosols (e.g. Haywood et al., 1997; Schult et al., 1997; Haywood and Ramaswamy, 1998; Myhre et al., 1998; Penner et al., 1998). A number of regional studies have been published. Many other global studies of direct forcing due to anthropogenic sulphate, black (elemental) carbon, carbonaceous and soot aerosols from biomass burning and fossil fuels, nitrate aerosols, soil dust and organic matter have been carried out (e.g. Boucher and Anderson, 1995; Chuang et al., 1997; Feichter et al., 1997; Hansen et al., 1997; Tegen et al., 1997; Li and Kou, 1998; Hansen et al., 1998; Miller and Tegen, 1998;

Penner et al., 1998; Stenchikov et al., 1998; Ackerman et al., 2000; Jacobson, 2001; Takemura et al., 2002, among others). Nevertheless, most of existing studies isolate particular aerosol types (e.g. Liousse et al., 1996), or combine either two types of aerosols (such as sulphate and carbonaceous aerosols, e.g. Jacobson 2001) or at best four aerosol species (carbonaceous, sulphate, soil-dust, sea-salt, e.g. Chin et al., 2000; Tegen et al., 2000; Takemura et al., 2002). Given the high spatial and temporal variability of atmospheric aerosols, unique aerosol types never occur in the atmosphere; in contrast, aerosol size distribution spectra are present as internal plus external mixtures of various aerosol components (Pruppacher and Klett, 1997). Such mixtures, along with complex aerosol properties, can only be simulated and represented by global aerosol models. The aerosol data used here are taken from the Global Aerosol Data Set (GADS, Koepke et al., 1997; http://www.meteo.physik.uni-muenchen.de/strahlung/aerosol.htm), which allows for ten aerosol components, representative of the atmosphere (see Section 3). Some recent studies combined model-generated different aerosol types, but they involve aerosol properties that are relatively limited in terms of the number of aerosol types or time scale (e.g. Chin et al., 2000; Tegen et al., 2000; Jacobson, 2001; Takemura et al., 2002). In addition, some of the existing studies consider fixed ambient relative humidity values, although relative humidity significantly affects the microphysical, optical and radiative properties of aerosols, and hence their direct SW radiative forcing, and there are important variations in water vapour with space and time (IPCC, 2001). Furthermore, some of the studies are performed on a regional scale (e.g. Podgorny et al., 2000) or over oceanic areas only (e.g. Penner et al., 2002), because the ocean albedo is relatively well characterized, and ocean areas are dark in the visible and near-infrared (near-IR), whereas substantial uncertainties exist for land surface albedos (Haywood et al., 1999), and the surface contribution to the reflected visible and near-IR is significantly larger than that contributed by aerosols. Recently, a long-term (1979–1992, 1996 to present) record of aerosol optical depth from TOMS observations was published (Torres et al., 2002) but for the near-ultraviolet (near-UV) (330–380 nm), while a product reduced to 0.55 μm is expected. Most of the above studies focus only on anthropogenic aerosols, while natural aerosols are equally important to climate. In addition, most of the existing studies are confined to the effect of aerosols on TOA SW radiation, though the role of aerosols is at least equally important to SW absorption by the atmosphere and the Earth's surface, as shown in this study. The reported global average estimates of the TOA direct aerosol forcing are highly uncertain in terms of magnitude and sign. The spread in the published forcing values is very large. Despite their generally acknowledged very important role in climate, and the significant progress that has been made during the last few years, the scientific level of understanding and confidence concerning aerosol direct radiative forcing remains very low (IPCC, 2001)

so that further studies are required. The objective of this study is to contribute towards this end.

A spectral radiative transfer model (Section 2) and radiative properties of aerosols, including surface and atmospheric parameters, was used here to compute the mean ultraviolet and visible clear-sky direct aerosol radiative forcing at TOA, within the atmosphere, and at the Earth's surface. Only the clear-sky direct forcing is considered here, as the other direct aerosol effect on SW radiation which takes place in the presence of clouds is considered to be smaller (Boucher and Anderson, 1995; Zhang et al., 1995; Haywood et al., 1997; Haywood and Ramaswamy, 1998) given the disparity in optical depths between aerosols and clouds, except for some cases (e.g. sulphate aerosols below cirrus clouds or soot aerosols above clouds, Highwood, 2000). Also, our focus is on the SW direct forcing, as the SW aerosol forcing is much larger than that of the thermal infrared (LW), except for some cases, such as mineral aerosols, for which the LW forcing can be as large as the SW one (e.g. Tegen et al., 1996). On a mean global basis, the LW aerosol forcing is estimated to be only 0.01 W m^{-2} (e.g. Haywood et al., 1997; Kondratyev, 1999). The cloudy-sky direct aerosol SW forcing, as well as the direct forcing in the near-infrared and thermal infrared will be investigated in future studies.

The aerosol radiative properties were computed based on detailed microphysical and optical properties (i.e. aerosol optical thickness, AOT, single-scattering albedo, ω_{aer}, and the asymmetry parameter, g_{aer}) taken from GADS. The aerosol optical properties are computed here by taking into account the effects of relative humidity, based on actual climatological data from the National Centers for Environmental Prediction (NCEP) and National Center for Atmospheric Research (NCAR) Global Reanalysis Project, and from the Tiros Operational Vertical Sounder (TOVS) data. The model computations for the aerosol radiative forcings were performed using actual climatological data for realistic surface and atmospheric constituent properties from existing comprehensive global climatological databases (e.g. NCEP/NCAR Global Reanalysis Project, TOVS, International Satellite Cloud Climatology Project, ISCCP-D2 series, Rossow and Schiffer, 1999), taking into account the global distribution of clouds, relative humidity and surface albedo. The study is performed on a global scale, on a 2.5° longitude–latitude pixel basis, and for winter and summer conditions, in order to detect regional and seasonal features of aerosol properties and forcings.

In Section 2, we describe the model and the methodology for modelling the aerosol radiative properties. The model input data are described in Section 3, while in Section 4 is given a detailed discussion of the derived aerosol properties used in the model. The model-computed forcings at TOA, within the atmosphere, and at the surface are given on a mean monthly 2.5° longitude–latitude pixel resolution for both winter and summer conditions (Section 5). Mean annual hemispherical and mean annual global

forcings are given in Section 6. The model results are discussed and compared with other estimates given in the literature.

2. The model

The deterministic spectral radiative transfer model used here was developed from a radiative–convective model (Vardavas and Carver, 1984). The mean monthly incoming total solar flux at TOA for each 2.5° latitude–longitude pixel, was computed by summing the corresponding mean daily flux on day n, given by

$$F_{\text{top}}^{\downarrow} = S_0 \mu_n d_n / r^2 \tag{1}$$

where μ_n is the cosine of the mean daily solar zenith angle, S_0 is the solar constant (1367 W m^{-2}, Frolich 1983), d_n is the daylength and $1/r^2$ is a correction factor due to the Earth's elliptical orbit. The daylength is given by

$$d_n = 8.64 \times 10^4 H_n / \pi \tag{2}$$

where the hour angle H_n is given by

$$H_n = \cos^{-1}(-\tan \theta \tan \delta_n) \tag{3}$$

with θ being the latitude of a given location on Earth and δ_n is the solar declination computed from

$$\delta_n = \arcsin(0.39779 \sin \lambda_n) \tag{4}$$

with

$$\lambda_n = L_n + 1.915 \sin g_n \tag{5}$$

$$L_n = 280.46 + K_n + 0.0077(\text{yr} - 2000) \tag{6}$$

$$g_n = 357.53 + K_n - 0.0095(\text{yr} - 2000) \tag{7}$$

$$K_n = 360(n - 1 + t/24)/365 \tag{8}$$

where yr is the year. The mean daily solar zenith angle is given by

$$\mu_n = A_n + B_n \sin H_n / H_n \tag{9}$$

with

$$A_n = \sin \theta \sin \delta_n \tag{10}$$

$$B_n = \cos \theta \cos \delta_n. \tag{11}$$

The computed incoming solar radiation at TOA has been compared successfully at TOA against scanner S4 data from the Earth Radiation Budget Experiment (ERBE, Barkstrom and Smith, 1986). The solar irradiance is computed at 115 wavelengths ranging from 0.20 to 0.85 μm, using the spectral profile of Thekaekara and Drummond (1971), normalized to a solar constant of 1367 W m^{-2}. For each wavelength, a set of monochromatic radiative flux transfer equations is solved for an absorbing/multiple-scattering atmosphere using the Delta-Eddington method of Joseph et al. (1976), which is an extension

of the Eddington method described in Shettle and Weinmann (1970) with the standard parameters g (asymmetry factor), τ (optical depth) and ω (single-scattering albedo) replaced by the following transformations:

$$\tau' = (1 - \omega f)\tau \tag{12}$$

$$\omega' = \frac{(1 - f)\omega}{1 - \omega f} \tag{13}$$

and

$$g' = \frac{g}{1 + g} \quad \text{with} f = g^2. \tag{14}$$

The atmosphere was divided into three layers for which the individual optical depths were evaluated from

$$\tau = \tau_{\text{aers}} + \tau_{\text{aera}} + \tau_{\text{ma}} + \tau_{\text{R}} \tag{15}$$

where τ_{aers} is the scattering aerosol optical depth, τ_{aera} is the absorption aerosol optical depth, τ_{ma} is that for molecular absorption and τ_{R} is that for Rayleigh scattering. The single-scattering albedo for each layer is

$$\omega = \omega_{\text{aer}} + \omega_{\text{R}} \tag{16}$$

where

$$\omega_{\text{aer}} = \tau_{\text{aers}}/\tau, \quad \omega_{\text{R}} = \tau_{\text{R}}/\tau \tag{17}$$

while

$$g = g_{\text{aer}}\omega_{\text{aer}} + g_{\text{R}}\omega_{\text{R}} \tag{18}$$

with g_{aer} being the aerosol asymmetry factor and $g_{\text{R}} = 0$. The first and second layers have ozone absorption and molecular Rayleigh scattering whilst the third layer, above a reflecting Earth's surface, has aerosol absorption/scattering and molecular scattering.

The direct effect of aerosols on the SW radiation (radiative forcing) denoted by ΔF henceforth, is considered here under clear-sky conditions only, since the aerosol optical depth values rarely exceed 1 on a mean monthly basis, i.e. they are much smaller than the corresponding cloud optical depth, by about one order of magnitude, except for specific cases, as explained in Section 1. Our study is confined to the UV–visible wavelengths and hence total aerosol forcing values are computed for the range 0.20–0.85 μm, from detailed spectral fluxes, with and without aerosols, computed at 115 wavelengths within the above spectral interval. In general, except for desert dust storm aerosols, the aerosol spectra are mainly composed of submicrometre-sized particles (typical size <0.5 μm, Jaenicke, 1993; Pruppacher and Klett, 1997) that can be treated independently of larger cloud particles (typical size <10 μm) in the Earth's radiation budget. With the exception of dust particles, the small size of aerosols, along with the rapid decrease of AOT with wavelength, support the study of the direct SW aerosol radiative forcing in the UV–visible range only, inducing a second-order direct effect in the thermal infrared (Haywood and Ramaswamy, 1998).

Reflection of incident solar radiation from the Earth's surface is taken into account. The surface reflectivity R_g for each 2.5°

resolution pixel was computed considering four types of surface: land, ocean, snow, and ice (frozen ocean). Then

$$R_g = f_{land} R_l + f_{ocean} R_o + f_{snow} R_s + f_{ice} R_i \qquad (19)$$

where f is the fraction of the Earth's surface covered by each type of reflecting surface. The ocean reflectivity R_o was computed using Fresnel reflection corrected for a non-smooth surface for an incidence angle $\phi = \cos^{-1} \mu$ from

$$R_o = 0.5 \left[\left(\frac{\sin \alpha}{\sin b} \right)^2 + \left(\frac{\tan \alpha}{\tan b} \right)^2 \right] + 0.016 \cos \phi \qquad (20)$$

where

$$\alpha = \phi - \sin^{-1}(\sin \phi / 1.333), \quad b = 2\phi - \alpha. \qquad (21)$$

For incident direct solar radiation on to a perfectly smooth water surface, the angle of reflection equals that of incidence, and for normal incidence the reflectivity is 0.024. For an ocean we have corrected the Fresnel reflectivity to take into account surface roughness which gives a higher reflectivity of about 0.04 for incident radiation normal to the surface (Kondratyev 1973). The correction factor $0.016 \cos \phi$ goes to zero when the radiation is parallel to the ocean surface to maintain a Fresnel reflectivity of unity in this case. Furthermore, we include the condition that if the Fresnel reflectivity is greater than the ice or snow reflectivity, which occurs at low solar elevations, then the reflectivities of both snow and ice are set equal to the Fresnel reflectivity. Kuhn (1989) gives observations that clearly show this behaviour for snow cover in Antarctica. The snow albedo was taken equal to 0.85 (Dickinson et al., 1993) while the sea-ice albedo was set equal to 0.55 (Roesch et al., 2002). Monthly average land-albedo values, which depend strongly on the type of land surface, were derived from ERBE as in Gupta et al. (1999).

The SW aerosol radiative forcing (ΔF), or more precisely the 'aerosol flux change', is the effect of aerosols on the SW radiation budget at TOA, at the Earth's surface, or within the atmosphere, and it is given by

$$\Delta F_i = F_i - F_{clear,i} \qquad (22)$$

where F_i and $F_{clear,i}$ are the SW radiative fluxes with and without the presence of aerosols, respectively. The index $-i$ involves various aerosol forcings defined in terms of the corresponding solar fluxes. The forcings ΔF_{TOA}, ΔF_{atmoab}, ΔF_{soldn} and $\Delta F_{netsoldn}$, represent the effect of aerosols on the outgoing solar radiation at TOA, the solar radiation absorbed within the atmosphere, the downward solar radiation at the Earth's surface, and the net downward (or absorbed) solar radiation at surface. The solar aerosol radiative forcings, ΔF_i, are computed by running the radiative transfer model with and without the aerosols included.

3. Model input data

3.1. Atmospheric molecules—absorption/scattering

The molecules considered in this study relevant to the 0.20–0.85 μm range of solar wavelengths were: O_3, temperature-dependent absorption in the Hartley–Huggins bands (0.20–0.35 μm), and absorption in the Chappuis bands (0.40–0.85 μm); O_2, Herzberg continuum (0.205–0.240 μm) absorption and scattering; N_2 scattering; and Ar scattering. The O_2 Herzberg data were taken from DeMore et al. (1997), as were the ozone cross-sections in the Hartley–Huggins bands at 273 K with a temperature correction as given in Vardavas and Carver (1984). For the Chappuis bands of ozone, the data of Griggs (1968) were used. The Rayleigh scattering due to atmospheric molecules is considered in the model in the way described by Vardavas and Carver (1984). The cross-section (cm^2) is given as

$$\sigma_R = 4.577 \times 10^{-21} \frac{\delta}{\lambda^4} [A(1 + B/\lambda^2)]^2 \qquad (23)$$

where λ is in μm, the coefficients A and B are tabulated in Allen (1976) for various molecules, while $\delta = (6 + 3\Delta)/(6 - 7\Delta)$, where Δ is the depolarization factor whose values are given in Table 1, together with the coefficients A and B for N_2, O_2 and Ar. For a mixture of atmospheric gases we obtain the Rayleigh cross-section from

$$\sigma_R = \sum_m \sigma_{Rm} n_m \qquad (24)$$

where n_m is the mixing ratio by volume, of molecules m.

The mean monthly values of total ozone-column abundance on 2.5° resolution were taken from the Television Infrared Observational Satellite (TIROS) Operational Vertical Sounder (TOVS) data, covering the years 1984–1993. The total atmospheric amounts for N_2, O_2 and Ar were partially distributed into each atmospheric layer according to its physical thickness as part of the total atmospheric column height. Surface topography was accounted for in this computation, by means of surface pressure taken from TOVS, in order to obtain the correct total atmospheric amount of each gas for the actual extent of the atmospheric column for a given pixel on the globe.

Table 1. Coefficients for computing the Rayleigh scattering cross-section (eq. 23)

Molecule	A	B	Δ
N_2	29.06×10^{-5}	7.70×10^{-3}	0.0305
O_2	26.63×10^{-5}	5.07×10^{-3}	0.0540
Ar	27.92×10^{-5}	5.60×10^{-3}	0.0320

3.2. Water vapour

The water vapour data used were taken from the NCEP/NCAR Global Reanalysis Project, which provides long-term (1948–continuing) climatological data. In particular, the pressure-level data for specific humidity, relative humidity, and temperature, for the years 1984 through 1993 (to match the ISCCP-D2 period) were used to compute the mean relative humidity of the aerosol layer.

3.3. Cloud cover

As suggested by other investigators (Takemura et al., 2002) an assumption of proper spatial and temporal distributions of clouds is necessary for proper estimations of the direct effect of aerosols, especially under clear-sky conditions, as attempted here. Thus, the aerosol forcing computations given in this study, were not simply performed by assuming clear-sky conditions for the whole pixel, but refer to the actual clear-sky part of the pixel, based on ISCCP data. Mean monthly data of cloud cover, A_c, for low, middle and high-level clouds were derived from the revised and improved latest series D2 of the ISCCP (accounting for 15 different cloud types including both liquid and ice phase, Rossow et al., 1996; Rossow and Schiffer, 1999) database for the years 1984–1993.

3.4. Surface reflection

The surface reflection is computed as explained in Section 2, by using surface-type cover fractions taken from ISCCP-D2, given on a mean monthly and 2.5° pixel resolution for the years 1984–1993, and their associated reflectivities, as in Hatzianastassiou and Vardavas (1999, 2001).

3.5. Surface pressure

A complete topography scheme is included in the model, which uses the TOVS-derived ISCCP surface pressure, gridded in 2.5 × 2.5 deg^2 pixels. Consideration of topography, instead of using the NCEP/NCAR 1000-mb level data, is important for regions well above sea-level, for the correct computation of the mean aerosol layer humidity (cf. Section 4), but also of the layer and total atmospheric amounts of the gases considered in this study.

3.6. Aerosol data

The model required aerosol radiative properties, AOT, ω_{aer} and g_{aer}, are directly related to the nature and chemical composition of the particles, which in turn depend on the location on the Earth. To perform the study, AOT data were taken from the Global Aerosol Data Set (GADS, Koepke et al., 1997). The dataset GADS is a completely revised version of the aerosol climatology compiled by d'Almeida et al. (1991) that has most

frequently been used (King et al., 1999), it consists of aerosol particle properties averaged over space and time, and it is currently used in climate models (e.g. Chin et al., 2002; Morcrette, 2002). Aerosol data from GADS are consistent in number distribution, mass per volume and optical properties, and comparable with different regional in situ and ground-based measurements and satellite data (Koepke et al., 1997). In GADS, the tropospheric aerosol particles are described by 10 main aerosol components, which are representative for the atmosphere and characterized through their size distribution and refractive index depending on the wavelength. These aerosol particles are based on components resulting from aerosol emission, formation and removal processes within the atmosphere, so that they exist as mixture of different substances, both external and internal. The GADS 10 aerosol components are: water insoluble, water soluble, soot, sea-salt accumulation mode, sea-salt coarse mode, mineral nucleation mode, mineral accumulation mode, mineral coarse mode, mineral transport mode, and sulphate (nucleation, accumulation, coarse and transport modes deal with size classes for sea-salt and mineral aerosols). For each aerosol component, the optical properties, i.e. the extinction, scattering, and absorption coefficients, single-scattering albedo, asymmetry factor, phase function and optical depth, are calculated using Mie theory at 61 wavelengths from 0.25 to 40 μm, and for eight values of relative humidity (0, 50, 70, 80, 90, 95, 98 and 99%), while visibility and Angstrom coefficient are also provided. The aerosol optical properties depend on the size, shape and composition of the particles, as well as on the ambient relative humidity. In general, Mie theory is applicable to homogeneous spherical particles (Liou, 1992). Therefore, if aerosol particles are not spherical, Mie theory, probably, would not be the best tool for computing the aerosol optical properties. However, at typical relative humidity values, many aerosol shapes are sphere-like. Although this is not so in arid and semi-arid regions, such as deserts, where non-sphericity remains an issue. To date, there is no reliable and operational technique to compute non-spherical aerosol particle optical properties for satellite applications (Ackerman 1997). Nevertheless, recent results presented by Takemura et al. (2000) show that differences in extinction efficiency factors between Mie particles and non-spherical particles do not exceed 20%; they are less than 5% in most cases. Tropospheric aerosols consist of particles of different origin. Thus, in GADS, the aerosol at a given location comprises various components, each with different particle number concentration (number per cm^3). This approach for modelling aerosol mixtures allows one to take into account the effects of relative humidity, which differ for each component in the mixture. The GADS global aerosol distribution is given as climatologically averaged values both for winter (December through February) and summer (June through August) seasons on a 5 × 5 deg^2 latitude–longitude resolution. The columnar aerosol properties are calculated on the basis of exponential aerosol height profiles (Jaenicke, 1993; Koepke et al., 1997; Hess et al., 1998). Observations confirm that the

concentration of aerosols decreases rapidly with increasing altitude, and that 80% of the total aerosol mass is contained below the lowest kilometre of the troposphere (Pruppacher and Klett 1997), except for polar aerosols.

The aerosol radiative properties are very sensitive to the ambient relative humidity, because it determines, along with the particle composition and the ambient temperature, the rate of condensation of water vapour on the surface of the particle, thereby determining the growth rate of the aerosol particle, and hence the particle size and refractive index. In GADS, the effect of the relative humidity on the aerosol properties is taken into account according to widely published formalisms (Hale and Querry, 1973; Hänel, 1976; Hänel and Zankl, 1979; Pruppacher and Klett, 1997).

Given the variability of aerosol microphysical, optical and radiative properties with relative humidity, it is essential to determine the actual relative humidity values for the aerosol layer, in order to estimate, as realistically as possible, aerosol particle properties from GADS, which are used here to compute aerosol radiative forcings. This was done in this study by using relative humidity values at eight levels in the atmosphere (surface, 925, 850, 700, 600, 500, 400 and 300 mb), as taken from the NCEP/NCAR Global Reanalysis Project for the years 1984–1993. Given that the NCEP/NCAR data are given for an adopted uniform surface pressure of 1000 mb, a complete topography scheme is included in the model (Hatzianastassiou et al., 2001), which uses surface pressure derived from the ISCCP-D2 TOVS package, gridded in 2.5×2.5 deg^2 pixels. Thus, the effective mean (computed by convoluting the relative humidity with altitude and the aerosol particle concentration decrease with height) relative humidity value was estimated, corresponding to the tropospheric aerosol layer extent.

4. Global distribution of mean monthly aerosol optical properties

From the 61 wavelengths of GADS, 11 fall within the UV–visible range of solar wavelengths used in this study. These are: 0.25, 0.35, 0.375, 0.4, 0.5, 0.55, 0.6, 0.65, 0.7, 0.75 and 0.8 μm. The spectral model computations are performed for 115 wavelengths from 0.20 to 0.85 μm. Thus, the model required AOT, ω_{aer} and g_{aer} on this wavelength grid were obtained through interpolation and extrapolation, when necessary. Finally, the solar radiative fluxes at TOA, within the atmosphere, and at the Earth's surface, were computed for each wavelength, with and without aerosols, which were then summed to yield the UV–visible radiative fluxes, and from their difference their radiative forcings (eq. 22). The GADS derived aerosol optical properties are given here for the wavelengths 0.25, 0.5 and 0.8 μm, as computed for the ambient aerosol layer humidity (Section 3) over the globe, for winter (January) and summer (July) conditions. The wavelength of 0.25 μm was chosen because it is the shortest GADS wavelength lying in the UV, whereas the visible wavelength of 0.5 μm is chosen because it is one of the WMO sunphotometer reference wavelengths, used in many studies (e.g. Chin et al., 2002) and surface measurements (AERONET, Holben et al., 2001), and because the spectrum of incoming solar radiation peaks strongly at this wavelength.

4.1. Aerosol optical thickness

In Fig. 1 we show the computed long-term global distribution of AOT. There is a general decrease with increasing wavelength, which is mainly attributed to water-soluble, soot and sulphate aerosol components (Koepke et al., 1997). Values of AOT are generally larger over land than over ocean (where they are generally smaller than 0.2), especially in areas with a high human population and a lot of pollution (e.g. Europe, North America, South and South-East Asia), but also over desert regions of the world (e.g. North Africa). High values of AOT are systematically located for both seasons over deserts as well as over the tropical Atlantic caused by the long-range transport of mineral particles. Over deserts, dust is the predominant aerosol component, except in the biomass-burning season (January) when carbonaceous aerosols are also important there, as also reported by Chin et al. (2002). Note that the area of higher AOT over the Atlantic is located about 10° northward in summer than in winter due to the changed atmospheric circulation, in agreement with satellite observations (e.g. Kaufman 1995). The largest AOT values in the northern mid-latitudes (40°–70°N) are associated with anthropogenic emissions involving various water insoluble and soluble (sulphates, nitrates) substances as well as black carbon in particulate matter. Indeed, most of the total aerosol mass enters the atmosphere at these latitudes (the latitudinal belt 30°–60°N contains about 88% of all anthropogenic sources for particulates). The AOT values are higher in northern subtropical latitudes during summer, in agreement with the model spatial distribution of AOT given by Jacobson (2001).

The AOT values for the Southern Hemisphere, are generally smaller than for the Northern Hemisphere, especially in the extratropical zones, because of a smaller land-to-sea ratio, given that the land is a more efficient source of particles than the ocean (Pruppacher and Klett, 1997). Higurashi et al. (2000) retrieved global distributions of AOT, for 4 months for the year 1990, from NOAA-11 AVHRR radiances at 0.5 μm, and validated them against selected stations of the AERONET sunphotometer dataset, which show larger average northern than southern values, by about 0.05, in agreement with our results, which globally and annually averaged, give a larger northern AOT by about 0.04. The GADS AOT values in biomass-burning areas, seem to be below the seasonal peak values of the order of 0.6–1.5 (at 0.5 μm) based on sunphotometer measurements (Holben et al., 2001). However, these values are subject to large temporal and spatial variation, which may limit their large-scale representativity.
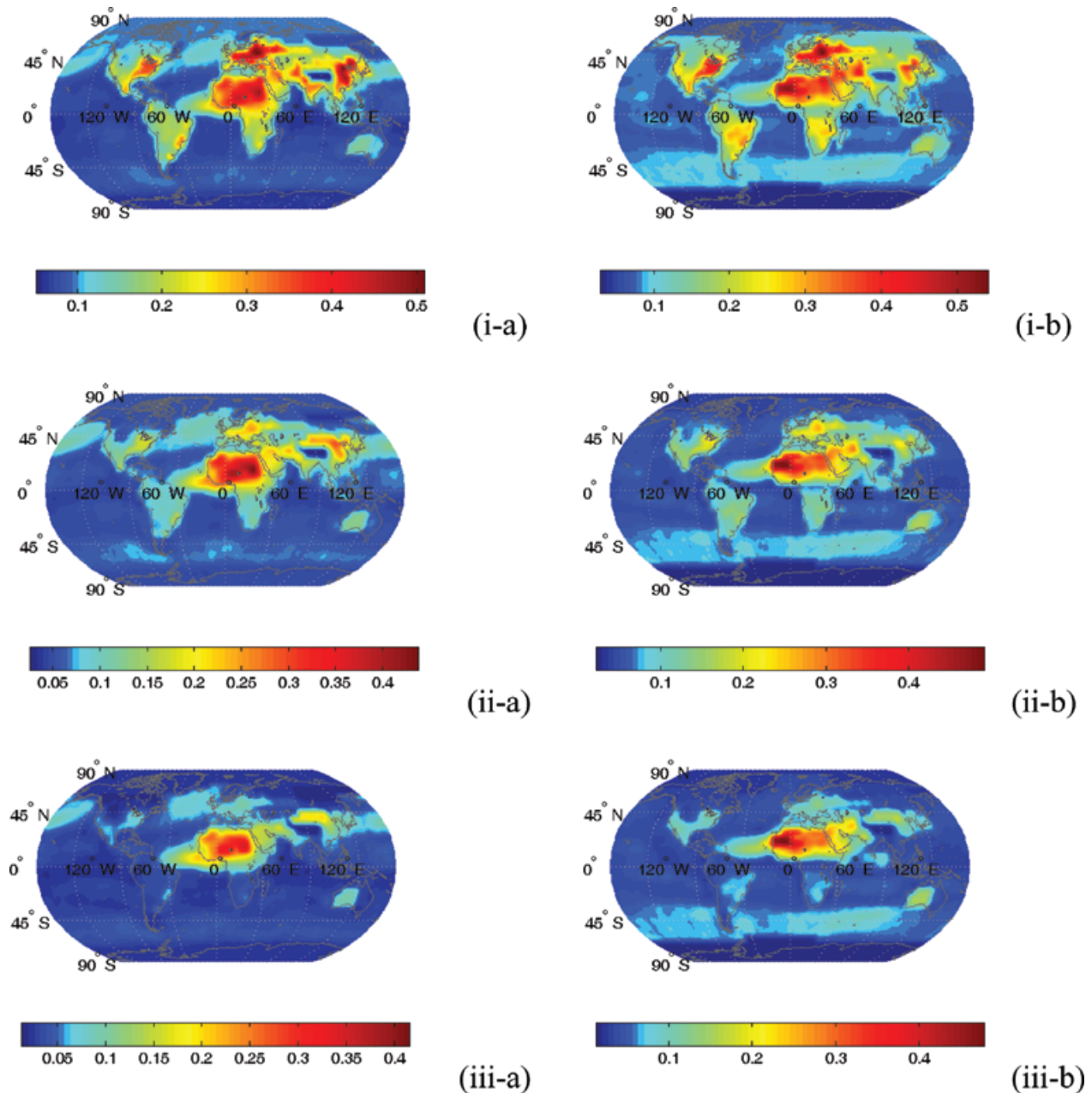
Fig 1. Global distribution of extinction aerosol optical thickness (AOT) at (i) 0.25 μm, (ii) 0.5 μm and (iii) 0.8 μm for (a) January and (b) July.

Our values seem to be closer to seasonal AOT peaks of 0.4–0.66, produced recently from a global transport model (Tegen et al., 1997). The transport of aerosol particles (mineral) from Northern Africa over the Atlantic Ocean (e.g. Swap et al., 1992; Chin et al., 2002) and over the Mediterranean (e.g. Dulac et al., 1992), but also from the Gobi desert over China to the Pacific (e.g. Zhang et al., 1993) is well reproduced. Large AOT values are also seen in the Arabian Peninsula and Gobi desert, as shown by other investigators (e.g. Takemura et al., 2002), but also by TOMS observations (Torres et al., 2002). Dust loads over Sahara

are more important in summer than in winter; this seasonal cycle of mineral dust aerosols, has also been reported by Torres et al. (2002) based on TOMS observations. Another feature is relatively high AOT values along the maritime band around 60°S, largely due to sea-salt particles, as also reported by Chin et al. (2002), by Penner et al. (2002), and found from Advanced Very High Resolution Radiometer (AVHRR-1) data at 0.63 μm as well. The AOT values are low over the polar regions, due to the small mass concentration of polar aerosols assumed in GADS (Koepke et al., 1997). Globally, our AOT values seem to provide

Table 2. Mean annual global and hemispherical long-term extinction aerosol optical thickness (AOT), aerosol single-scattering albedo (ω_{aer}) and aerosol asymmetry parameter (g_{aer}) derived from the Global Aerosol Data Set for actual atmospheric and surface conditions at wavelengths 0.25, 0.5 and 0.8 μm

	North	South	Globe
AOT (0.25 μm)	0.15	0.09	0.12
AOT (0.5 μm)	0.1	0.06	0.08
AOT (0.8 μm)	0.07	0.05	0.06
ω_{aer} (0.25 μm)	0.87	0.95	0.91
ω_{aer} (0.5 μm)	0.94	0.98	0.96
ω_{aer} (0.8 μm)	0.95	0.98	0.97
g_{aer} (0.25 μm)	0.76	0.76	0.76
g_{aer} (0.5 μm)	0.72	0.74	0.73
g_{aer} (0.8 μm)	0.72	0.74	0.73

a generally encouraging qualitative comparison with preliminary global distributions of AOT from MODIS measurements on the NASA EOS Terra spacecraft (Ramanathan et al., 2001; Kaufman et al., 2002). Thus, it reproduces the observed transport of coarse dust from Africa, the fine particles in pollution from North America, Europe and South and South-East Asia, but also the salt particles in the windy Southern Hemisphere (see Kaufman et al., 2002).

Mean annual global values of AOT are found to be equal to 0.08 at 0.5 μm (Table 2), lower than values from a global transport model (Tegen et al., 2000) including many aerosol types, which range from about 0.1 to 0.12 for the period 1950–1990, showing an increasing trend. Our value is close to 0.082 given by Tegen et al. (1997). Takemura et al. (2002) using a global three-dimensional model including carbonaceous, sulphate, soil-dust and sea salt aerosols, have given an annual global mean AOT value equal to 0.116. A globally and annually averaged AOT value (at 0.55 μm) given by Ramanathan et al. (2001) is equal to 0.12 ($\pm$0.04). Our mean annual global AOT value of 0.08, results from mean annual hemispherical values of 0.1 and 0.06 for the Northern and Southern Hemisphere, respectively; the corresponding values given by Takemura et al. (2002), including four aerosol types, are equal to 0.16 and 0.07 (at 0.55 μm). Chin et al. (2002) using the Georgia Institute of Technology-Goddard Global Ozone Chemistry Aerosol Radiation and Transport (GO-CART) model, which includes the same four aerosol types as Takemura et al., have given separate estimates of AOT at 0.5 μm for each aerosol type, which combined give a total mean annual global estimate of AOT equal to 0.14. Our estimated mean annual global and hemispherical AOT values exhibit a significant spectral variation (Table 2). Thus, in the UV, the mean global AOT equals 0.12, while it drops down to 0.06 towards the near-IR.

4.2. Aerosol single-scattering albedo

Global distribution of single-scattering albedo, ω_{aer}, is given in Fig. 2 for three different wavelengths in the UV–visible range. The ω_{aer} values range from about 0.65 to 1, with higher values over oceanic areas that indicate sulphate aerosols originating from oceanic DMS (dimethylsulphide) and sea salt, and lower ω_{aer} values over land. In particular, ω_{aer} values as low as 0.65 (at 0.25 μm), associated with dust particles, are found over deserts (Sahara, Arabia, Kalahari, Gobi), which are characterized by strongly absorbing mineral aerosols (e.g. minerals). These results seem to agree with other global aerosol models (e.g. Takemura et al., 2002) or TOMS observations (Herman et al., 1997). Note that ω_{aer} values over deserts increase with increasing wavelength (e.g. ω_{aer} at 0.8 μm is equal to about 0.92 over the Sahara) due to the decreasing imaginary part of the complex refractive index of mineral components. Low ω_{aer} values over oceanic areas, such as the tropical Atlantic, western Pacific (off the Asian coast) or Mediterranean, indicate transport of mineral aerosols originating from desert areas (e.g. trade winds in tropical Atlantic). Small ω_{aer} values, down to about 0.8, are also found over areas characterized by soot and water insoluble components, such as Europe, North and South America, South, and South-East Asia or central Africa. Water insoluble particles have continental, but no desert, origin and they stay near their sources, which are industries, ash, dust from fields and streets, pollen or spores (Koepke et al., 1997). They occur largely over regions of agriculture activities. Soot is produced by combustion processes, such as industries, home heating, traffic and biomass burning. This explains the low ω_{aer} values over densely populated regions of northern mid latitudes during the local winter (Fig. 2). From the northern industrialized regions, soot is transported during winter months to the Arctic, which can be seen in low ω_{aer} values in the Arctic (north of 60°N) during winter. These particles are observed as an Arctic haze (Heintzenberg and Leck, 1994). The 'polluted' aerosol particles originate from agricultural and industrialized areas of Eurasia, Japan and North America's mid latitudes, which are transported within the Arctic air masses (Shaw et al., 1993), under favourable synoptic situations and atmospheric general circulation, where they persist especially during winter to spring under a stable polar vortex, before this breaks down in summer. In contrast, strongly scattering aerosol particles ($\omega_{aer} > 0.95$) are found in Antarctica, indicating significant composition from sulphate and sea salt, rather than minerals (Koepke et al., 1997; Hess et al., 1998), against low ω_{aer} values (close to 0.9) as shown by Takemura et al. (2002), and close to 0.97, as given by Jacobson (2001). Observations at Amundsen Scott (90°S) indicate ω_{aer} values of 0.965 (Heintzenberg et al., 1997). High values of ω_{aer} in Antarctica, are due to a very small land-to-sea ratio and homogeneous ocean coverage in the mid latitudes of the Southern Hemisphere. The emission sources of solar absorbing aerosols are less intense and extensive in the Southern Hemisphere (e.g. South America's and Africa's forest fires) and their transport to
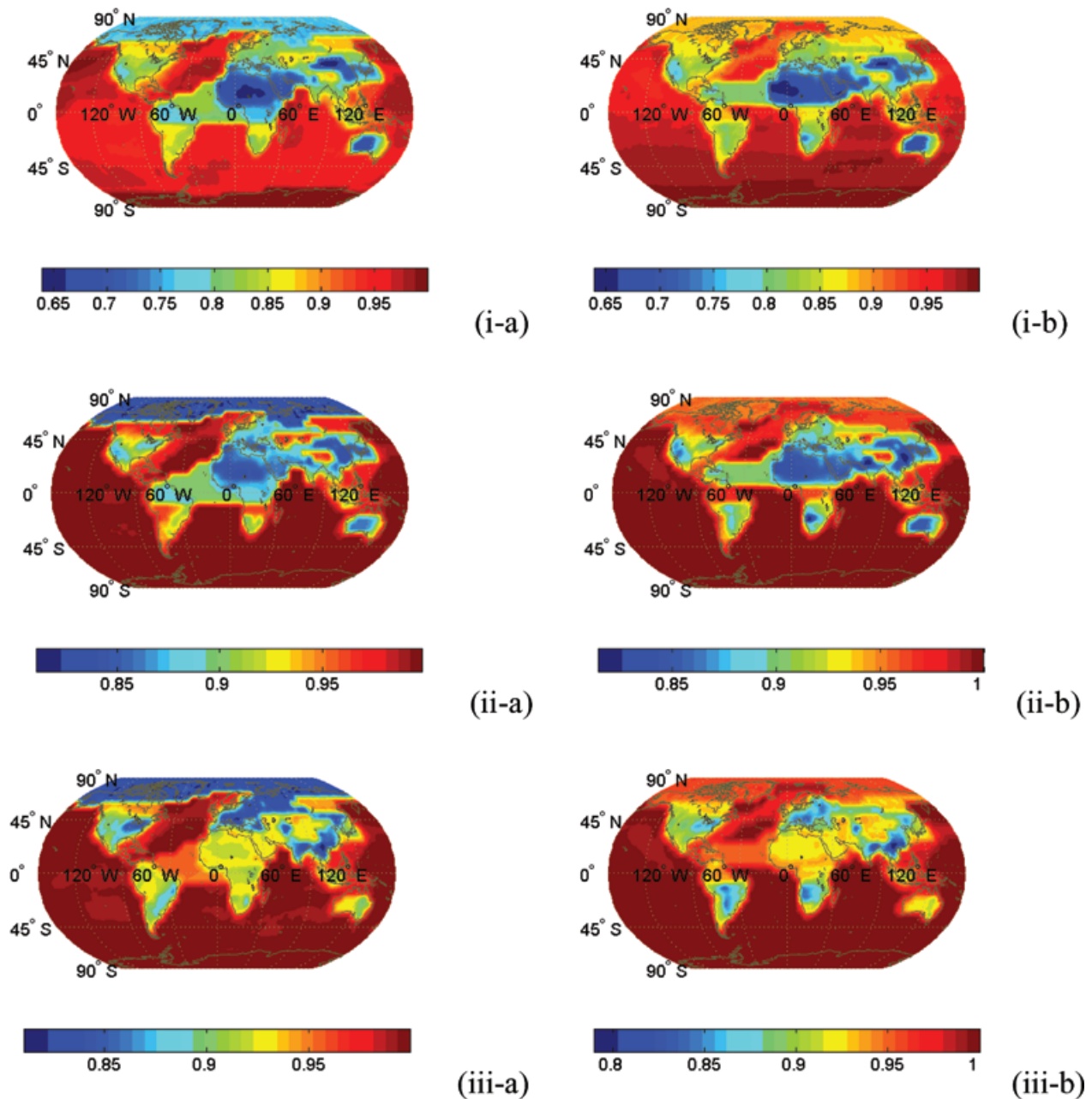
Fig 2. Global distribution of aerosol single-scattering albedo at (i) 0.25 μm, (ii) 0.5 μm and (iii) 0.8 μm for (a) January and (b) July.

polar latitudes is not helped by the synoptic situation and atmospheric dynamics. GADS seems to represent rather satisfactorily the site of biomass-burning areas (South Africa, South America), which are characterized by highly absorbing aerosols during the local dry season, with ω_{aer} values as low as 0.85, especially at 0.8 μm, during that season. Values there are between 0.8 and 0.9 as indicated by the Smoke, Clouds, and Radiation-Brazil Project (SCAR-B) experiment (Hobbs et al., 1997a). Our values seem to agree with those presented by Takemura et al. (2002), and presumably with AERONET measurements, based on comparisons

made between Takemura model products and AERONET and other observations as well.

Jacobson (2001) displayed yearly averaged model-estimated ω_{aer} values at 0.55 μm, equal to 0.89 and 0.94 for the Northern and Southern Hemisphere, respectively, against our corresponding values of 0.94 and 0.98 (at 0.5 μm), i.e. their values seem to be lower than ours, although in both cases the southern hemispherical ω_{aer} values are found to be smaller than the northern ones, by about 0.04. On the other hand, the corresponding values given by Takemura et al. (2002) show a smaller inter-hemispherical

difference 0.02, resulting from values of 0.92 and 0.94 for the Northern and Southern Hemisphere, respectively. Haywood and Ramaswamy (1998) have reported a mean annual global ω_{aer} value equal to 0.93, but for black carbon and anthropogenic sulphate aerosols only. The same authors indicate that including sulphate aerosols from natural sources, and other aerosol types such as dust, organic carbon and nitrates, would result in higher ω_{aer} values. Our mean annual hemispherical and global ω_{aer} values seem to be higher than those of others. This should be due to the fact that GADS includes both natural and anthropogenic

aerosols, which are modelled using multiple aerosol components that are not always taken into account by other models (usually limited up to four components). At 0.25 μm, the mean ω_{aer} values for the Northern and the Southern Hemisphere, are equal to 0.87 and 0.95, resulting in a mean global value of 0.91.

4.3. Aerosol asymmetry parameter

The global distribution of the asymmetry factor, g_{aer}, is shown in Fig. 3 with values varying between about 0.6 and 0.85,
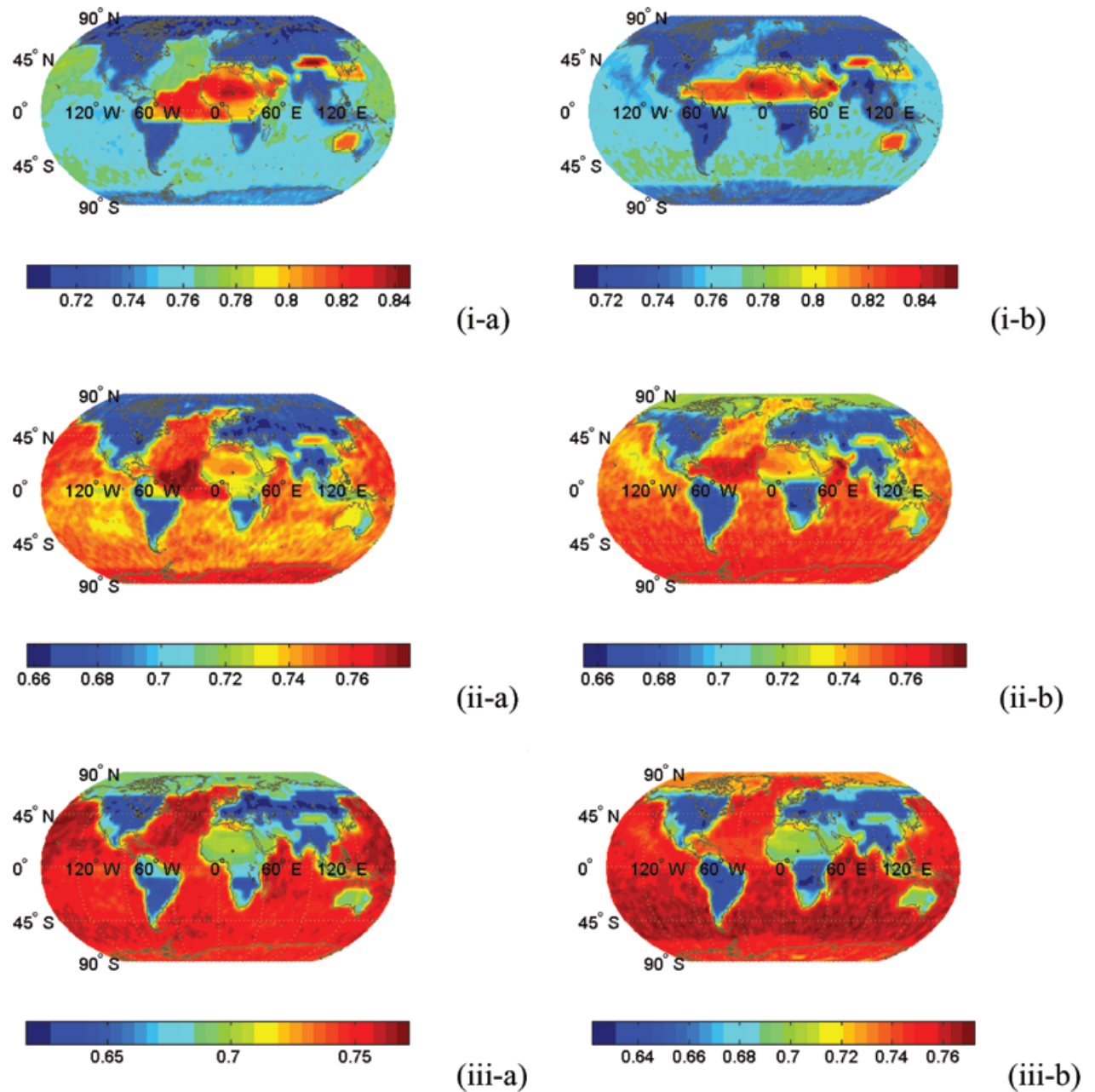

Fig 3. Global distribution of aerosol asymmetry parameter at (i) 0.25 μm, (ii) 0.5 μm and (iii) 0.8 μm for (a) January and (b) July.

indicating a prevailing forward scattering for aerosols in the uv-visible range. Our values fall within the range of values given by Haywood et al. (1999) and IPCC, (2001) for various aerosol types. Model-computed yearly averaged g_{aer} values given by Jacobson (2001), are equal to 0.68 and 0.71 for the Northern and Southern Hemisphere, respectively, against our corresponding values of 0.72 and 0.74. The asymmetry parameter, g_{aer}, is larger for the Southern Hemisphere than for the Northern Hemisphere, especially poleward of 30°, implying a larger forward scattering in the southern than in the northern middle and high latitudes, as also indicated by the results of Jacobson (2001). Our estimated global visible g_{aer} value of 0.73 (0.5 μm), is lower than the corresponding UV g_{aer} value of 0.76.

5. Global distribution of mean monthly aerosol forcings

The computed total UV–visible mean monthly (winter and summer) pixel (2.5° longitude–latitude) aerosol forcings are given in terms of outgoing solar radiation at TOA (ΔF_{TOA}), solar atmospheric absorption (ΔF_{atmoab}), downwelling solar radiation at the surface (ΔF_{soldn}), net downward or absorbed solar radiation at the surface ($\Delta F_{netsoldn}$) in W m^{-2}.

5.1. Aerosol forcing ΔF_{TOA}

In general, aerosols increase, through reflection, the outgoing solar radiation at TOA, by up to 6 W m^{-2} on a mean monthly basis, thus producing a planetary cooling (Fig. 4). However, aerosols can produce a planetary warming by decreasing the outgoing solar radiation at TOA, by up to 4 W m^{-2}. This is due to important absorption of atmospheric solar radiation by aerosol particles, such as those characterized by mineral components, over desert areas (e.g. the Sahara, Arabia) or soot particles over continental areas (e.g. Europe, North Asia, North America). In general, the sign of the effect of aerosols on the outgoing SW radiation at TOA (aerosol forcing ΔF_{TOA}) under a clear sky is determined by the values of ω_{aer}, AOT and surface albedo, R_g. Thus, whereas planetary warming is found over Siberia in winter, there is planetary cooling in summer. The role of R_g is also shown by the contrast between the planetary cooling produced by mineral aerosols over oceanic areas of low R_g or over continental areas of R_g lower than 0.3 (sub-Sahel), and the planetary warming produced by similar mineral aerosols over highly reflecting deserts ($R_g > 0.3$). The aerosol-induced planetary warming over the highly reflecting surfaces (e.g. polar regions) is due to particle absorption caused by polluted aerosols (haze), which is increased through multiple reflections between ice- or snow-covered surfaces and the aerosols above. This aerosol effect has been investigated by many scientists (e.g. Blanchet 1989; Charlson et al., 1992; Haywood and Shine, 1997; Myhre et al., 1998) and it was recently verified by field measurements during the Aerosol Characterization

Experiment (ACE-2) by Vitale et al. (2000). An example is the Arctic haze containing a considerable amount of anthropogenic impurities, including soot (originating from the industrialized centres in northern Europe, North America and Asia, and undergoing long-range transport by winter anti-cyclonic conditions, Brock et al. (1989)) that decrease the albedo substantially and act against global cooling due to anthropogenic sulphates. The Arctic aerosol type, including soot particles transported from mid-latitude continental areas, can be found north of 70°N (Fig. 2). The anticyclonic situation, favourable for this transport, persists mainly during winter through springtime, when an intense high-pressure system pushes the Arctic front to the south. Large polluted agricultural and industrialized areas of Eurasia, Japan and North America are then within the Arctic air mass, which can move aerosols across the North Pole. This atmospheric activity is further amplified by the lack of clouds and precipitation. Note that our model does not reproduce planetary warming over the Kali and Australian deserts, despite the small ω_{aer} values there, possibly due to relatively low GADS AOT values there, but also due to relatively lower surface albedo values (0.2–0.25, against values up to 0.4 over Sahara or Arabia). This shows the importance of surface albedo below the aerosols, apart from ω_{aer}, in determining the sign of ΔF_{TOA}. Also, our model computations indicate planetary cooling by up to 1.5 W m^{-2} off the western coast of South Africa in July, lower than values of more than 5 W m^{-2} given by Takemura et al. (2002). This is due to the fact that GADS does not provide large AOT values over these areas (Fig. 1), as shown by satellite observations in the near-UV (Torres et al., 2002), which needs to be improved. The largest forcing ΔF_{TOA} values are found in tropical and subtropical latitudes. The magnitude of ΔF_{TOA} is determined by the incoming solar radiation, the reflectance of the aerosol layer, directly associated with AOT, and the clear-sky fraction. The maximum summer tropical and subtropical ΔF_{TOA} values are associated with relatively small cloud cover (e.g. over India in January and over the Mediterranean in July), and large incoming solar radiation values, along with relatively large AOT values. The ΔF_{TOA} values in mid latitudes of the Northern Hemisphere (Europe, USA) are larger in summer than in winter, mainly because of larger incoming solar fluxes at TOA and less cloudiness during this season.

5.2. Aerosol forcing ΔF_{atmoab}

A significant aerosol-induced increase in solar atmospheric absorption can be seen in Fig. 5, where aerosols are found to cause increases as large as 25 W m^{-2} in areas (e.g. Sahara) characterized by significant amounts of absorbing aerosols (such as mineral-dust) over surfaces with a large surface albedo (>0.3). The solar atmospheric absorption is also found to be increased by less than 10 W m^{-2}, due to aerosols, over Europe, North America, South and South-East Asia, but also over South Africa, the
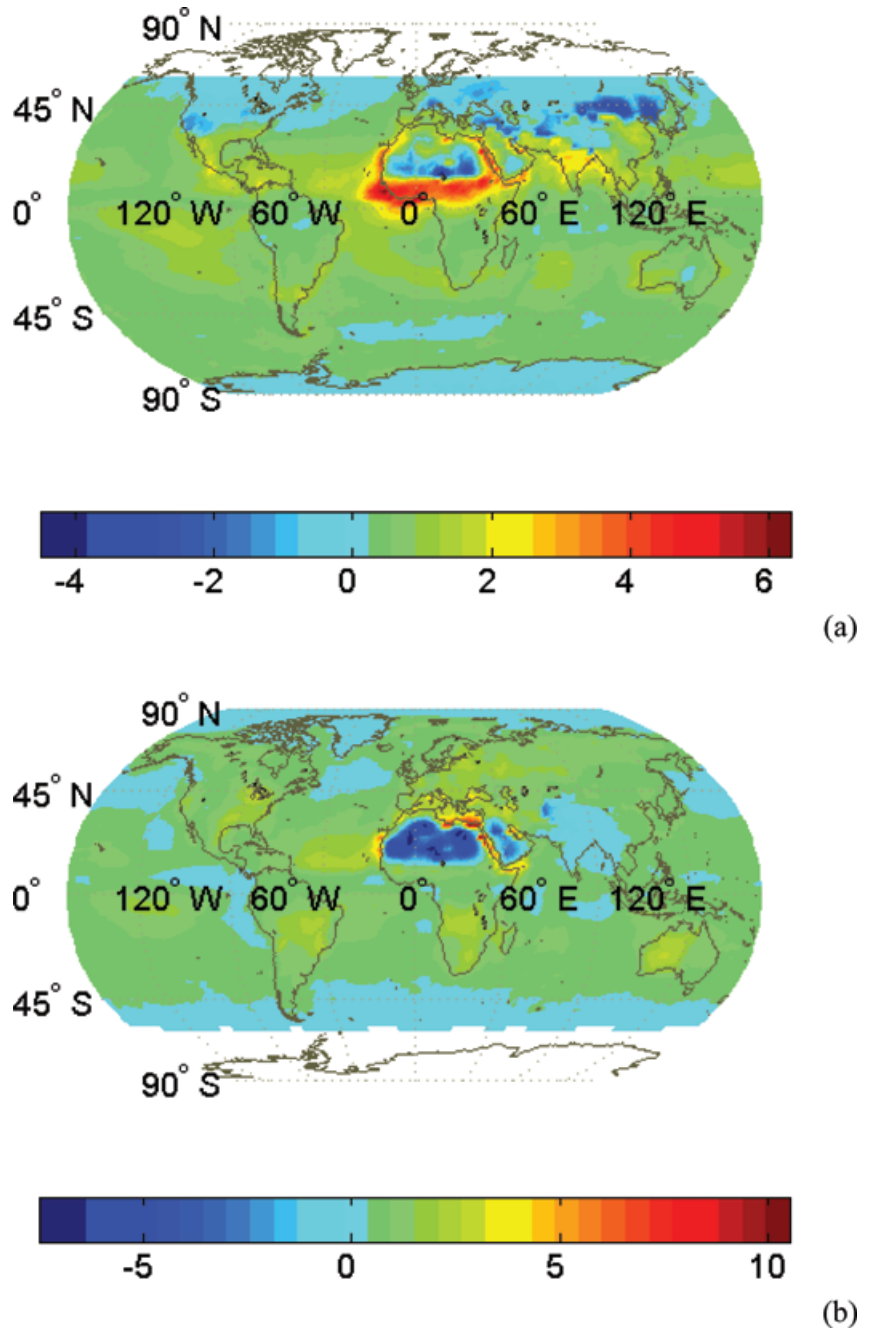
Fig 4. Global distribution of the aerosol effect on the outgoing UV–visible radiation at top-of-atmosphere (aerosol forcing ΔF_{TOA}, W m^{-2}) for (a) January and (b) July.

Amazon basin and Australia. Note that our model computations indicate a significant aerosol-induced solar atmospheric absorption of 5–10 W m^{-2} in the sub-Sahelian region (5°–10°N) in January, which is the local dry season. This indicates that GADS represents rather satisfactorily absorbing aerosols in this case, since (Wild, 1999) according to the Global Fire Atlas (Arino and Molinette, 1998), fires are largely concentrated in the area between 5°N and 10°N in the Northern Hemisphere winter (January). Of course, the values of the effect of aerosols on the SW

atmospheric absorption (ΔF_{atmoab}) in the sub-Sahelian region can also be attributed to desert dust advected from the Sahara southwards towards the equator, through the 'harmattan' trade winds occurring in the dry season. In contrast, during the Northern Hemisphere summer (July), with the dry season shifted to the Southern Hemisphere, the biomass burning is dominant to the south of the equator, with maximum concentration between 5°S and 15°S. Our model computations indicate (Fig. 5) an aerosol-induced increase in solar atmospheric absorption during summer,
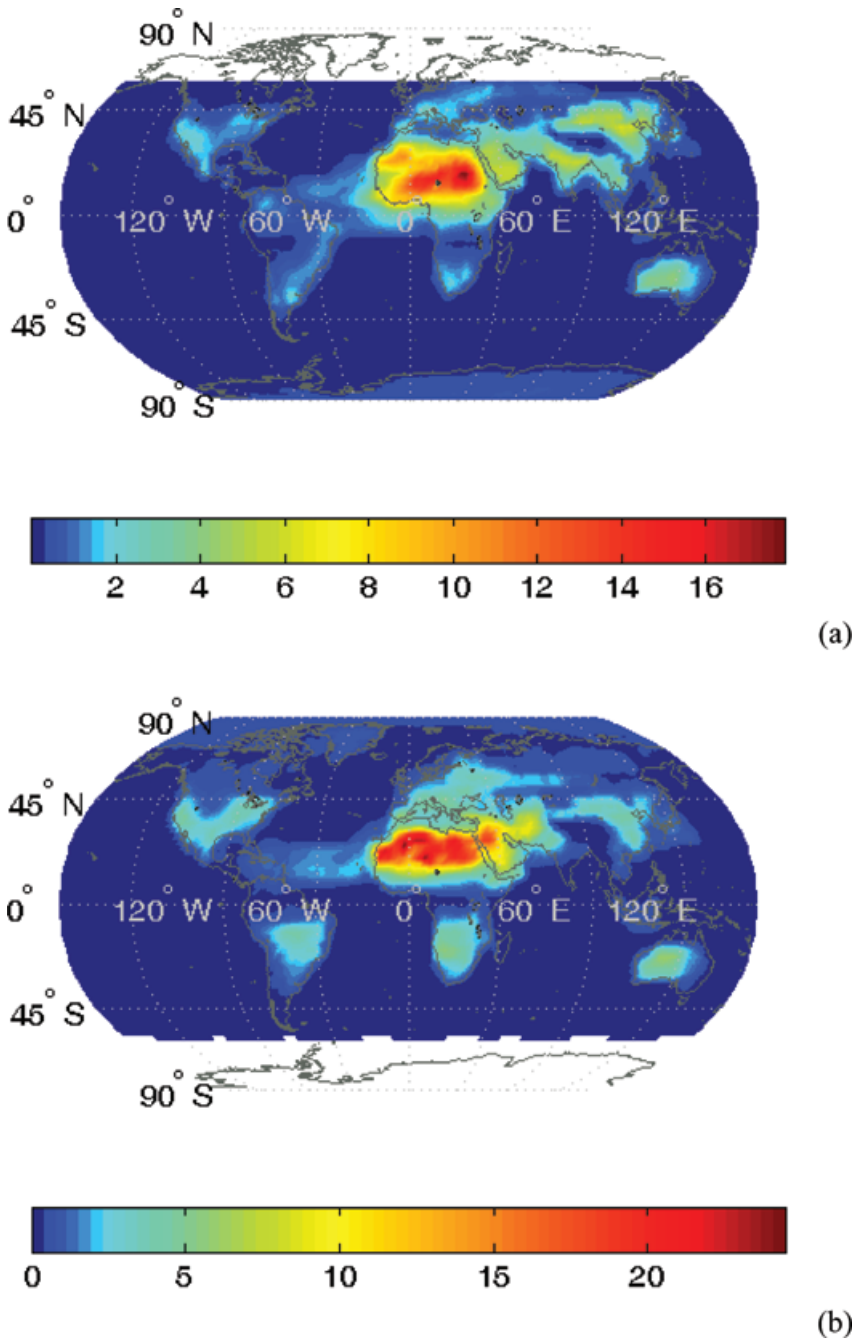
Fig 5. Global distribution of the aerosol effect on the atmospheric absorption of UV–visible radiation (aerosol forcing ΔF_{atmoab}, W m^{-2}) for (a) January and (b) July.

of about 5–8 W m^{-2} in South Africa and within the Amazon basin.

5.3. Aerosol forcings ΔF_{soldn} and $\Delta F_{netsoldn}$

Our model results (Figs. 6 and 7) indicate that aerosols can decrease regionally the downward mean UV–visible radiation at the Earth's surface by up to 28 W m^{-2}, and the absorbed solar radiation by the surface by as much as 23 W m^{-2}, thus producing a very important surface radiative cooling. The largest decreases in surface solar radiation are found over areas with significant aerosol amounts (AOT); thus, AOT, ΔF_{soldn} and $\Delta F_{\text{netsoldn}}$ values are correlated. Therefore, a large effect of aerosols on the downward solar radiation at the surface (ΔF_{soldn}) is encountered over land areas (especially over deserts) while smaller forcing values are found over oceans, due to optically thin aerosol
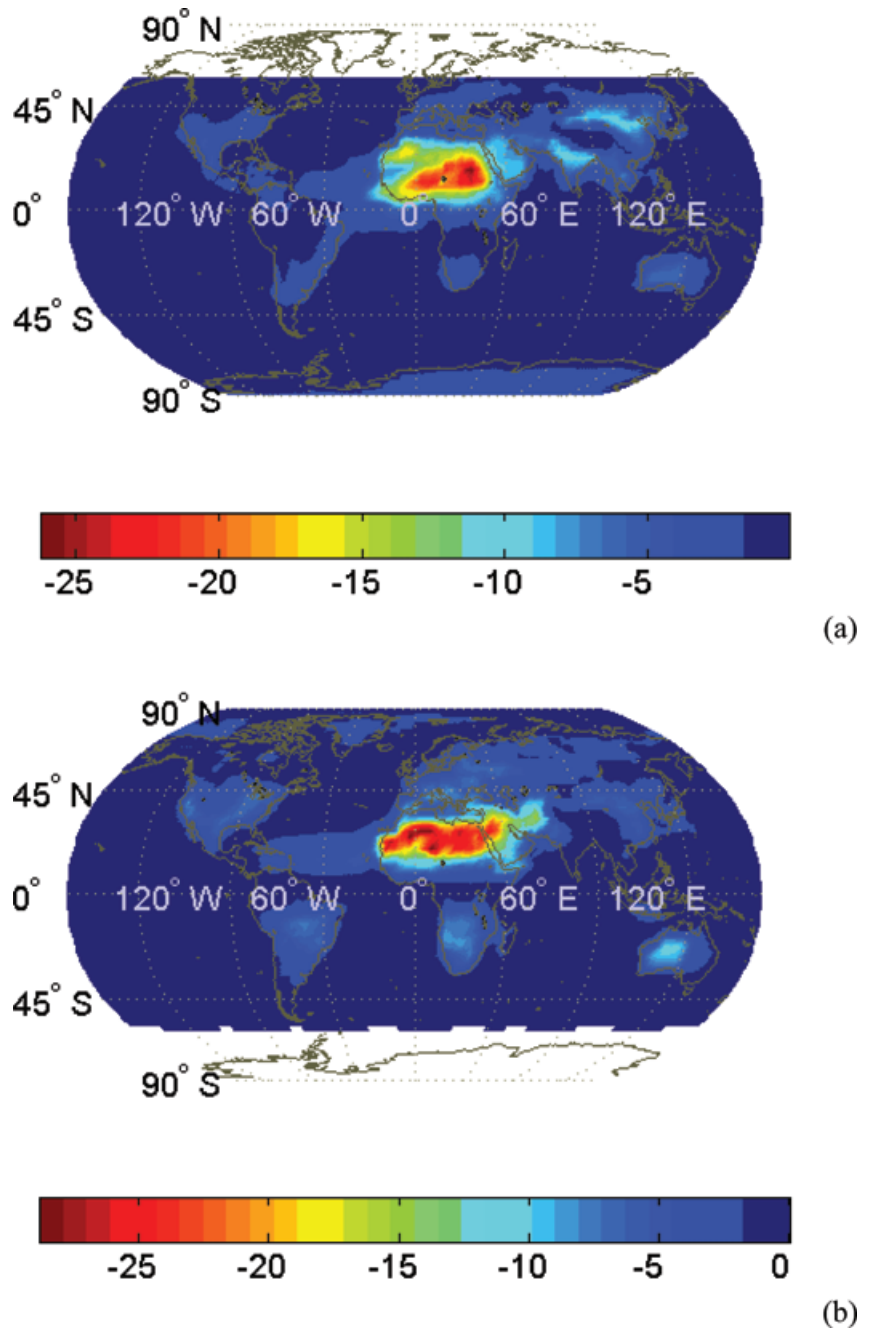
Fig 6. Global distribution of the aerosol effect on the downward UV–visible radiation at the Earth's surface (aerosol forcing ΔF_{soldn}, W m^{-2}) for (a) January and (b) July.

layers above. According to our model computations, aerosols can produce locally an effect on solar surface radiation that is up to three times larger than their effect at TOA, as also reported by Kaufman et al. (2002) for smoke aerosols, and by Ramanathan et al. (2001). This is also in agreement with the factor of 2.7 given by Lelieveld et al. (2002) from aerosol radiative forcing computations based on measurements of the Mediterranean Intensive Oxidation Study, performed in summer 2001 in Crete (Greece). Lelieveld et al., reported a ΔF_{soldn} value of 18 W m^{-2}, but on a mean daily basis, which rather supports our computed

mean monthly value of about 9 W m^{-2}. Note that our result refers to a mean monthly AOT value equal to 0.15 and an ω_{aer} value of 0.87, against daily values of 0.21 and 0.87, respectively, given by Lelieveld et al., The radiative effect of aerosols on the absorbed solar radiation at the Earth's surface is determined by the forcing ΔF_{soldn} and the surface albedo R_g. Therefore, the features of $\Delta F_{netsoldn}$ are similar to those of ΔF_{soldn}, except in the high-albedo polar regions. Note that in cases of small ΔF_{atmoab} values, the forcings ΔF_{TOA} and $\Delta F_{netsoldn}$ are almost equal in magnitude. Under such circumstances, the aerosol
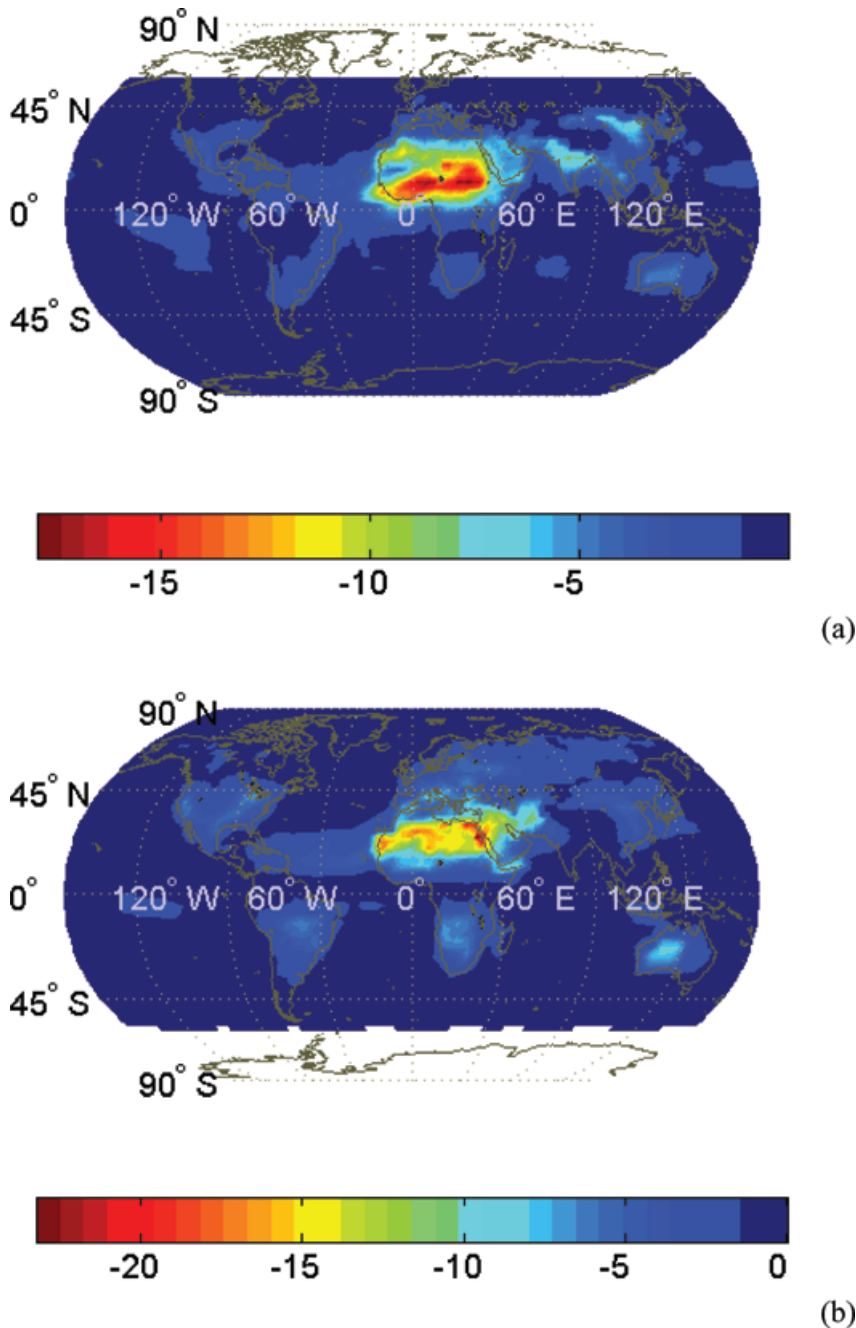
Fig 7. Global distribution of the aerosol effect on the absorbed UV–visible radiation by the Earth's surface (aerosol forcing $\Delta F_{\text{netsoldn}}$, W m^{-2}) for (a) January and (b) July.

forcing at the surface could be estimated from their corresponding forcing at TOA, as suggested by Ramanathan et al. (2001), for purely scattering aerosols.

6. Mean annual hemispherical and mean annual global aerosol forcings

Table 3 displays the model-computed clear-sky visible direct aerosol solar radiative forcings together with estimates from other studies. Many of the existing results in the literature do not provide all the components of the aerosol forcings (ΔF_{TOA}, ΔF_{atmoab}, ΔF_{soldn} or $\Delta F_{\text{netsoldn}}$), while most of them give estimates for specific aerosol types, which need to be combined in order to yield the total aerosol effect. Also, some studies are limited to oceanic regions only. Few recent works give global estimates of the total direct aerosol forcing, most of them only at TOA, neither at the surface nor within the atmosphere. As far as it concerns specific aerosol-type forcings, only a few representative values are given in Table 3, whereas a large number of other estimates exist in the literature. Note that our values were

Table 3. Mean annual global and hemispherical (NH, SH) clear-sky total UV–visible direct aerosol radiative forcing (ΔF_i in W m^{-2}). Forcings are given in terms of: outgoing solar radiation at TOA (ΔF_{TOA}), atmospheric absorption of solar radiation (ΔF_{atmoab}), downward solar radiation at surface (ΔF_{soldn}), and net downward solar radiation at surface ($\Delta F_{netsoldn}$). Estimates of the global annual average shortwave indirect aerosol forcing, and of the global annual average total forcing of greenhouse gases are also given, based on IPCC-2001

	ΔF_{TOA}	ΔF_{atmoab}	ΔF_{soldn}	$\Delta F_{netsoldn}$
Present (Globe)	0.61	0.83	−1.86	−1.44
Present (NH)	0.62	1.43	−2.74	−2.05
Present (SH)	0.60	0.23	−0.99	−0.83
Takemura et al. (2002)	1.29[g] (0.23[h])			
Jacobson (2001)	1.23		−4.0	
Tegen et al. (2000)[e]	−0.12 − 0.51			
Haywood et al. (1999)	1.57			
Cusack et al. (1998)	2.26			−6.81
Hansen et al. (1998)	0.42			
Penner et al. (1998)[f]	0.30–0.75			
Harshvardhan (1993)	1.5–3.0			
Penner et al. (1992)	>2			
Coakley and Cess (1985)	3 ± 0.5	−0.27 ± 0.18		−4.4 ± 0.5
IPCC-2001 (sulphate)	0.2–0.8			
IPCC-2001 (biomass burning)	0.07–0.6			
IPCC-2001 (black carbon)	−0.1−−0.4			
IPCC-2001 (organic carbon)	0.03–0.3			
IPCC-2001 (mineral dust)	−0.4–0.6			
Harvey (2000)[a,c]	0.28–0.66			
Haywood et al. (1999)[d]	3.0–6.5			−7.4−−10.8
Penner et al. (1998)[a,b]	0.49–0.88	1.31–2.11		
Myhre et al. (1998)[a,c]	0.26–0.95			
Hobbs et al. (1997b)[b]	<0.3			
Charlson et al. (1992)[a]	1.3			
Charlson et al. (1991)[a]	1.02			
Indirect effect (IPCC, 2001)	2.1			
Greenhouse effect (IPCC, 2001)	2.43 ± 10%			

[a] Only sulphate particles.
[b] Only carbonaceous particles.
[c] Values from various sources in literature.
[d] Only for oceanic regions.
[e] No biomass-burning aerosols included.
[f] Internal mixture of aerosols.
[g] For clear-sky conditions only.
[h] For overcast conditions only.

computed using data for natural plus anthropogenic aerosols from GADS, and for actual surface and atmospheric conditions, e.g. actual cloud cover fractions and surface albedo. This makes a difference to the other results.

In general, aerosols act to increase both the reflection of solar radiation at the Earth's TOA, and the absorption of solar radiation within the atmosphere, while they result in a decrease of the downward and the absorbed solar radiation at the Earth's surface. Among these separate radiative effects, the largest one is found to be at the surface, irrespective of the hemisphere. The mean annual global forcing $\Delta F_{netsoldn}$ is about equal to or even larger than twice the forcings ΔF_{TOA} and ΔF_{atmoab}. It is worth noting that

significant differences in the relative importance of the forcings at TOA, atmosphere and at the surface, are found between the two hemispheres. For example, the ratio $\Delta F_{netsoldn}/\Delta F_{atmoab}$ is about −1.4 in the Northern Hemisphere and −3−−6 in the Southern Hemisphere. This indicates a much larger aerosol effect on atmospheric absorption of solar radiation in the Northern Hemisphere compared with the Southern Hemisphere.

7. Summary and conclusions

A spectral radiative transfer model was developed, for estimating the clear-sky total ultraviolet and visible direct effect of natural

plus anthropogenic aerosol particles, in terms of aerosol forcings, using existing climatological data. Apart from other input data, the model requires aerosol optical properties, namely, the aerosol optical depth, the single-scattering albedo and the asymmetry parameter, to yield spectral (0.2–0.85 μm) and total solar radiative fluxes at TOA, within the atmosphere, and at the Earth's surface, with and without aerosols, in order to compute aerosol forcings. The radiative forcing computations were performed using complete and comprehensive globally distributed data for surface and atmospheric key parameters, such as the surface albedo, cloud cover and specific humidity. Global distributions of aerosol optical properties were computed by using aerosol data from the Global Aerosol Data Set based on actual global relative humidity values for the atmospheric aerosol layer.

In general, AOT values are larger in the Northern Hemisphere compared with the Southern Hemisphere, especially in the northern mid-latitude densely populated and polluted continental areas (e.g. Europe, North America, South and South-East Asia), associated with a larger land-to-sea ratio and anthropogenic emissions, but also over desert regions (e.g. Northern Africa, Arabian peninsula, Gobi, Kalahari deserts). The annually and globally averaged AOT value is equal to 0.08 at 0.5 μm, with an inter-hemispherical difference equal to 0.04, resulting from 0.1 and 0.06, the values for the Northern and the Southern Hemisphere, respectively. The global annual AOT values at 0.25 and 0.8 μm are equal to 0.12 and 0.06, respectively. The aerosol single-scattering albedo is found to vary between 0.65 and values near 1, with a mean annual global value of 0.96 at 0.5 μm and 0.91 at 0.25 μm. Larger southern hemispherical ω_{aer} values were found, associated with the larger southern ocean coverage, with highly scattering sea-salt particles. Values of ω_{aer} as low as 0.65 are found over desert areas, due to mineral components, as well as over industrialized world regions (North America, Europe, South and South-East Asia) due to soot components. Low ω_{aer} values are found in the Arctic in winter, associated with 'polluted' aerosols (Arctic haze) that are transported from industrialized continental mid latitudes of the Northern Hemisphere, whereas a transport of mineral aerosols from deserts over oceanic areas is found, resulting in relatively low ω_{aer} values.

Our model results show that under clear skies, natural plus anthropogenic aerosols generally increase the mean UV–visible outgoing radiation at TOA (through scattering), inducing a planetary cooling. Regionally, they can cause significant planetary warming (by up to 5 W m^{-2}) over desert and polar regions with relatively high surface albedo, as well as over northern mid-latitude continents in winter, due to particle absorption of solar radiation. The aerosols are found to increase the solar absorption significantly within the atmosphere, by up to 20–25 W m^{-2}, in cases of high amounts of absorbing aerosols and strongly reflecting surfaces underneath (e.g. Sahara). On the other hand, aerosols reduce regionally the surface downward and absorbed solar radiation, by up to 28 W m^{-2}, especially in areas with high amounts of aerosol or significantly absorbing particulate matter,

producing thus a surface radiative cooling with important ramifications for evaporation, and hence precipitation, at the regional scale. The aerosol-induced increase in solar atmospheric absorption may partly explain the systematic underestimation of SW atmospheric absorption by models compared to measurements (e.g. Wild, 1999), also known as the 'absorption paradox', which is also related to large deviations between model computations and measurements of surface SW radiation budgets.

Mean annual hemispherical estimates of direct aerosol forcings computed with our model, show larger values in the Northern Hemisphere compared with the Southern Hemisphere, by factors ranging from 1 to 6 for the various aerosol forcings (ΔF_{TOA}, ΔF_{atmoab}, ΔF_{soldn} and $\Delta F_{\text{netsoldn}}$). On a mean annual global basis, aerosols are found to increase the reflected UV–visible radiation at TOA by 0.6 W m^{-2} (planetary cooling) and the atmospheric absorption of solar radiation by 0.8 W m^{-2} (atmospheric warming), while they decrease the solar radiation reaching the Earth's surface by 1.9 W m^{-2}, and the surface-absorbed solar radiation by 1.4 W m^{-2} (surface cooling), showing a larger radiative effect at the surface compared with the atmosphere. Thus, aerosols could decrease the vertical atmospheric temperature gradient, changing the atmospheric circulation, and probably reduce evaporation, cloud formation and precipitation (Kaufman et al., 2002).

The results of our study indicate that rather than studying the aerosol direct radiative effect at TOA, it is more important to evaluate and quantify the distribution of this effect within the atmosphere and at the surface, since these can counteract (heating versus cooling, respectively) and give the same total result through different combinations. Changes in the ratio of these two separate effects may be critical for climate change. Unfortunately, such changes might not be detected at TOA (from satellites), since the two opposing effects can counteract and result in a small or even zero effect at TOA. Models remain as the only alternative. Nevertheless, in specific cases where aerosols are almost purely scattering, the aerosol effects at the surface could be detected at TOA. Although global warming due to greenhouse gases should exceed the global cooling effect of aerosols, on the regional scale aerosol cooling could become dominant; therefore, evaluation and study of aerosol radiative forcings at a regional level is necessary. To this end, an extensive work is in preparation, aimed at detecting regional patterns in aerosol radiative forcings (e.g. for the Mediterranean Basin). In that work, apart from GADS, other global aerosol climatological data from satellite observations (e.g. MODIS, MOD_08 M3 and TOMS at 550 nm) that become gradually available will be used and the aerosol properties will be compared against data from improved surface-based networks (AERONET), ensuring more complete and precise aerosol radiative properties and forcings. However, since no one system is yet capable of providing totally unambiguous information on aerosol size distribution, the single-scattering albedo and the asymmetry parameter (King et al., 1999), except for some validated TOMS ω_{aer} data for local studies only, use of

aerosol data from the above sources will be restricted to aerosol optical thickness.

8. Acknowledgments

References

Ackerman, S. A. 1997. Remote sensing aerosols using satellite infrared observations. *J. Geophys. Res.* **102**, 17 069–17 079.

Ackerman, S. A., Toon, O. B., Stevens, D. E., Heymsfield, A. J., Ramanathan, V. and Welton, E. 2000. Reduction of tropical cloudiness by soot. *Science* **288**, 1042–1047.

Allen, C. W. 1976. *Astrophysical Quantities* 3rd edn. Athlone Press, London.

Arino, O. and Molinette, J.-M. 1998. The 1993 Africa Fire Map, cover page. *Int. J. Remote Sens.* **19**, 2019–2023.

Barkstrom, B. and Smith, G. 1986. The Earth radiation budget experiment – science and implementation. *Rev. Geophys.* **24**, 379–390.

Blanchet, J.-P. 1989. Toward an estimation of climatic effects due to Arctic aerosols. *Atmos. Environ.* **23**, 2609–2625.

Boucher, O. and Anderson, T. L. 1995. General circulation model assessment of the sensitivity of direct climate forcing by anthropogenic sulfate aerosols to aerosol size and chemistry. *J. Geophys. Res.* **100**, 26 117–26 134.

Brock, C. A., Radke, L. F., Lyons, J. H. and Hobbs, P. V. 1989. Arctic hazes in summer over Greenland and the North American Arctic. I. Incidence and origins. *J. Atmos. Chem.* **9**, 129–148.

Charlson, R. J., Langner, J., Rodhe, H., Leovt, C. and Warren, S. 1991. Perturbation of the Northern Hemisphere radiative balance by backscattering from anthropogenic sulfate aerosols. *Tellus* **43AB**, 152–163.

Charlson, R. J., Schwartz, S. E., Hales, J. M., Cess, R. D., Coakley, J. A., Jr., Hansen, J. E. and Hofmann, D. J. 1992. Climate forcing by anthropogenic aerosols. *Science* **255**, 423–430.

Chin, M., Jacob, D. J., Gardner, G. M., Spiro, P. A., Foreman-Fowler, M. and Savoie, D. L. 2000. A global three-dimensional model of tropospheric sulfate. *J. Geophys. Res.* **101**, 18 667–18 690.

Chin, M., Ginoux, P., Kine, S., Torres, O., Holben, B. N., Duncan, B. N., Martin, R. V., Logan, J. A., Higurashi, A. and Nakajima, T. 2002. Tropospheric aerosol optical thickness from the GOCART model and comparisons with satellite and Sun photometer measurements. *J. Atmos. Sci.* **59**, 461–483.

Chuang, C. C., Penner, J. E., Taylor, K. E., Grossmann, A. S. and Walton, J. J. 1997. An assessment of the radiative effects of anthropogenic sulfate. *J. Geophys. Res.* **102**, 3761–3778.

Coakley, A., Jr, and Cess, R. 1985. The two-stream approximation in radiative transfer. Including the angle of the incident radiation. *J. Atmos. Sci.* **32**, 409–418.

Coakley, A., Jr, Cess, R. D. and Yurevich, F. B. 1983. The effect of tropospheric aerosols on the Earth's radiation budget: A parameterization for climate models. *J. Atmos. Sci.* **40**, 116–138.

Cusack, S., Slingo, A., Edwards, J. M. and Wild, M. 1998. The radiative impact of a simple aerosol climatology on the Hadley Center atmospheric GCM. *Q. J. R. Meteorol. Soc.* **124**, 2517–2526.

D'Almeida, G. A., Koepke, P. and Shettle, E. P. 1991. *Atmospheric Aerosols: Global Climatology and Radiative Characteristics*. Deepak, Hampton, VA, 560 pp.

DeMore, W. B., Sander, S. P., Golden, D. M., Hampson, R. F., Kurylo, K. J., Howard, C. J., Ravishankara, A. R. and Molina, M. J. 1997. *Chemical Kinetics and Photochemical Data for Use in Stratospheric Modeling*, Evaluation 12, JPL Publ. 97-4, 266 pp.

Deuzé, J. L., Herman, M., Goloub, P., Tanré, D. and Marchand, A. 1999. Characterization of aerosols over ocean from POLDER/ADEOS1. *Geophys. Res. Lett.* **26**, 1421–1424.

Dickinson, R., Henderson-Sellers, A. and Kennedy, P. 1993. *Biosphere-Atmosphere Transfer Scheme (BATS) Version 1e as coupled to the NCAR Community Climate Model. Tech. Note NCAR/TN-387+STR* National Center for Atmospheric Research, Boulder, CO.

Dulac, F., Tanré, D., Bergametti, G., Buat-Ménard, P., Desbois, M. and Sutton, D. 1992. Assessment of the African airborne dust over the western Mediterranean Sea using Meteosat data. *J. Geophys. Res.* **97**, 2489–2506.

Feichter, J., Lohmann, U. and Schult, I. 1997. The atmospheric sulfur cycle in ECHAM-4 and its impact on the shortwave radiation. *Climate Dyn.* **13**, 235–246.

Fouquart, Y., Bonnel, B. and Ramaswamy, V. 1991. Intercomparing shortwave radiation codes for climate studies. *J. Geophys. Res.* **96**, 8955–8968.

Frolich, C. 1983. Data on total and spectral solar irradiance. *Comments Appl. Opt.* **22**, 3928.

Griggs, M. 1968. Absorption coefficients of ozone in the ultraviolet and visible regions. *J. Chem. Phys.* **49**, 857–859.

Gong, S. L., Barrie, L. A., Blanchet, J.-P. and Spacek, L. 1998. Modeling size-distributed sea salt aerosols in the atmosphere: An application using Canadian climate models. In: *Air Pollution Modeling and Its Applications XII* (eds S.-E. Gryning and N. Chaumerliac). Plenum Press, New York.

Gupta, S.-K., Ritchey, N. A., Wilber, A. C., Whitlock, C., Gibson, G. G. and Stackhouse, P. W. 1999. A climatology of surfae radiation budget derived from satellite data. *J. Climate* **12**, 2691–2710.

Hale, G. M. and Querry, M. R. 1973. Optical constants of water in the 200 nm to 200 μ m wavelength region. *Appl. Opt.* **12**, 555–563.

Hänel, G. 1976. The properties of atmospheric aerosol particles as functions of the relative humidity at thermodynamic equilibrium with the surrounding moist air. *Adv. Geophys.* **19**, 73–188.

Hänel, G. and Zankl, B. 1979. Aerosol size and relative humidity: Water uptake by mixtures of salts. *Tellus* **31**, 478–486.

Hansen, J., Sato, M. and Ruedy, R. 1997. Radiative forcing and climate response. *J. Geophys. Res.* **102**, 6831–6864.

Hansen, J., Sato, M., Lacis, A., Ruedy, R., Tegen, I. and Matthews, E. 1998. Climate forcings in the industrial era. *Proc. Natl. Acad. Sci., USA* **95**, 12 753–12 758.

Harshvardhan, J. 1993. Aerosol-climate interactions. In: *Aerosol–Cloud–Climate Interactions* (ed P. Hobbs). Academic, San Diego, CA, 76–95.

Harvey, L. D. D. 2000. Constraining the aerosol radiative forcing and climate sensitivity. An editorial comment. *Clim. Change.* **44**, 413–418.

Hatzianastassiou, N. and Vardavas, I. 1999. Shortwave radiation budget of the Northern Hemisphere using International Satellite Cloud Climatology Project and NCEP/NCAR climatological data. *J. Geophys. Res.* **104**, 24 401–24 421.

Hatzianastassiou, N. and Vardavas, I. 2001. Shortwave radiation budget of the Southern Hemisphere using ISCCP C2 and NCEP/NCAR climatological data. *J. Climate,* **14**, 4319–4329.

Hatzianastassiou, N., Cleridou, N. and Vardavas, I. 2001. Polar cloud climatologies from ISCCP C2 and D2 datasets. *J. Climate* **14**, 3851–3862.

Haywood, J. M. and Ramaswamy, V. 1998. Global sensitivity studies of the direct radiative forcing due to anthropogenic sulfate and black carbon aerosols. *J. Geophys. Res.* **103**, 6043–6058.

Haywood, J. M. and Shine, K. P. 1997. Multi-spectral calculations of the direct radiative forcing by anthropogenic sulfate and fossil-fuel soot aerosols. *Q. J. R. Meteorol. Soc.* **123**, 1907–1930.

Haywood, J. M., Roberts, D. L., Slingo, A., Edwards, J. M. and Shine, K. P. 1997. General circulation model calculations of the direct radiative forcing by anthropogenic sulfate and fossil-fuel soot aerosol. *J. Climate* **10**, 1562–1567.

Haywood, J. M., Ramaswamy, V. and Soden, B. J. 1999. Tropospheric aerosol climate forcing in clear-sky satellite observations over the oceans. *Science* **283**, 1299–1303.

Heintzenberg, J. and Leck, C. 1994. Seasonal variation of the atmospheric aerosol near the top of the marine boundary layer over Spitsbergen related to the Arctic sulphur cycle. *Tellus* **46B**, 52–67.

Heintzenberg, J., Charlson, R. J., Clarke, A. D., Liousse, C., Ramanathan, V., Shine, K. P., Wendisch, M. and Helas, G. 1997. Measurements and modeling of aerosol single scattering albedo: progress, problems, and prospects. *Beitr. Phys. Atmos.* **70**, 249–263.

Herman, J. R., Barthia, P. K., Torres, O., Hsu, C., Seftor, C. and Celarier, E. 1997. Global distributions of UV-absorbing aerosols from Nimbus7/TOMS data. *J. Geophys. Res.* **102**, 16 911–16 923.

Hess, M., Koepke, P. and Schult, I. 1998. Optical properties of aerosols and clouds: Te software package OPAC. *Bull. Am. Meteorol. Soc.* **79**, 831–844.

Highwood, E. J. 2000. Effect of cloud inhomogeneity on direct radiative forcing due to aerosols. *J. Geophys. Res.* **105**, 17 843–17 852.

Higurashi, A., Nakajima, T., Holben, B. N., Smirnov, A., Frouin, R. and Chatenet, B. 2000. A study of global aerosol optical climatology with two-channel AVHRR remote sensing. *J. Climate* **13**, 2011–2027.

Hobbs, P. V., Reid, J. S., Herring, J. D., Nance, J. D., Weiss, R. E., Ross, J. L., Hegg, D. A., Ottmar, R. D. and Liousse, C. A. 1997a. Particle and trace-gas measurements in the smoke from prescribed burns of forest products in the Pacific Northwest. In: *Biomass Burning and Global Change* (ed. J. S. Levine). MIT Press, Cambridge, MA, 697–715.

Hobbs, P. V., Reid, J. S., Kotchenrither, R. A., Ferek, R. J. and Weiss, R. 1997b. Direct radiative forcing by smoke from biomass burning. *Science* **275**, 1776–1778.

Holben, B. N. and co-authors. 2001. An emerging ground-based aerosol climatology: Aerosol optical depth from AERONET. *J. Geophys. Res.* **106**, 12 067–12 097.

Intergovernmental Panel on Climate Change (IPCC), 2001. In: *Climate Change 2001: The Scientific Basis* (eds J. T. Houghton et al). Cambridge University Press, New York, 881 pp.

Jacobson, M. Z. 2001. Global direct radiative forcing due to multicomponent anthropogenic and natural aerosols. *J. Geophys. Res.* **106**, 1551–1568.

Jaenicke, R. 1993. Tropospheric aerosols. In: *Aerosol–Cloud–Climate Interactions* (ed.P. Hobbs). Academic, San Diego, CA, 1–31.

Jones, A., Roberts, D. L. and Slingo, A. 1994. A climate model study of the indirect radiative forcing by anthropogenic sulfate aerosols. *Nature* **370**, 450–453.

Joseph, J. H., Wiscombe, W. J. and Weinmann, J. A. 1976. The Delta-Eddington approximation of radiative flux transfer. *J. Atmos. Sci.* **33**, 2452–2459.

Kahle, A. B. and Deirmendjan, D. 1973. The black cloud experiment. *Rep. R-1263-ARPA*, Rand, Santa Monica, CA.

Kaufman, Y. J. 1995. Remote Sensing of direct and indirect aerosol forcing. In: *Aerosol Forcing of Climate* (edsR. J. Charslon and J. Heintzenberg). Dahlem Workshop, *Environm. Sci. Res.* Report 17. Wiley, Chichester, 297–332.

Kaufman, Y. J., Tanré, D., Gordon, H. R., Nakajima, T., Lenoble, J., Frouin, R., Grassl, H., Herman, B. M., King, M. D. and Teillet, P. M. 1997. Passive remote sensing of tropospheric aerosol and atmospheric correction for the aerosol effect. *J. Geophys. Res.* **102**, 16 815–16 830.

Kaufman, Y. J., Tanré, D. and Boucher, O. 2002. A satellite view of aerosols in the climate system. *Nature* **419**, 215–223.

Kiehl, J. T. and Briegleb, B. P. 1993. The relative roles of sulfate aerosols and greenhouse gases in climate forcing. *Science* **260**, 311–314.

Kiehl, J. T., Schneider, T. L., Rasch, P. J., Barth, M. C. and Wong, J. 2000. Radiative forcing due to sulfate aerosols from simulations with the National Center for Atmospheric Research Community Climate Model, Version 3. *J. Geophys. Res.* **105**, 1441–1457.

King, M. D., Kaufmann, Y. J., Tanré, D. and Nakajima, T. 1999. Remote sensing of tropospheric aerosols from space: Past, present, and future. *Bull. Am. Meteorol. Sos.* **80**, 2229–2259.

Koepke, P., Hess, M., Schult, I. and Shettle, E. P. 1997. *Global Aerosol Data Set.* Report No 243, Max-Planck Institut für Meteorologie. Hamburg, Germany, 44 pp.

Kondratyev, K. Y. 1973. *Radiation Characteristics of the Atmosphere and the Earth's Surface.* Amerind, New Delhi.

Kondratyev, K. Y. 1999. *Climatic Effects of Aerosols and Clouds.* Springer, New York, 264 pp.

Kuhn, M. H. 1989. The role of land ice and snow in climate. In: *Understanding Climate Change, Geophys. Monogr. Ser., Vol. 52* (eds. A. Berger, R. E. Dickinson, and J. W. Kidson). American Geophysical Union, Washington, DC, 17–28.

Langner, J. and Rodhe, H., 1991. A global three-dimensional model of the tropospheric sulfur cycle. *J. Atmos. Chem.* **13**, 225–263.

Lelieveld, L. and co-authors 2002. Global air pollution crossroads over the Mediterranean. *Science* **298**, 794–799.

Li, Z. and Kou, L. 1998. The direct radiative effect of smoke aerosols on atmospheric absorption of visible sunlight. *Tellus* **50B**, 543–554.

Li, X., Maring, H., Savoie, D., Voss, K. and Prospero, J. M. 1996. Dominance of mineral dust in aerosol light-scattering in the North Atlantic trade winds. *Nature* **380**, 416–419.

Liou, K. N. 1992. *Radiation and Cloud Processes in the Atmosphere, Theory, Observation and Modelling*. Oxford University Press, New York, 487 pp.

Liousse, C., Penner, J. E., Chuang, C., Walton, J. J., Eddleman, H. and Cachier, H. 1996. A global three-dimensional model study of carbonaceous aerosols. *J. Geophys. Res.* **101**, 19 411–19 432.

Miller, R. L. and Tegen, I. 1998. Climate response to soil dust aerosols. *J. Climate* **11**, 3247–3267.

Morcrette, J.-J. 2002. The surface downward longwave radiation in the ECMWF forecast system. *J. Climate* **15**, 1875–1992.

Myhre, G., Stordal, F., Restad, K. and Isaksen, I. S. A. 1998. Estimation of the direct radiative forcing due to sulfate and soot aerosols. *Tellus*, **50B**, 463–477.

Penner, J. E., Dickinson, R. E. and O'Neill, C. A. 1992. Effects of aerosols from biomass burning on the global radiation budget. *Science* **256**, 1432–1433.

Penner, J. E., Chuang, C. C. and Grant, K. 1998. Climate forcing by carbonaceous and sulfate aerosols. *Climate. Dyn.* **14**, 839–851.

Penner, J. E., Zhang, S. Y., Chin, M., Chuang, C. C., Feichter, J., Feng, Y., Georgdzhayev, I. V., Ginoux, P., Herzog, M., Higurashi, A., Koch, D., Land, C., Lohmann, U., Mischenko, M., Nakajima, T., Pitari, G., Soden, B., Tegen, I. and Stowe, L. 2002. A comparison of model and satellite-derived aerosol optical depth and reflectivity. *J. Atmos. Sci.* **59**, 441–460.

Podgorny, I. A., Conant, W., Ramanathan, V. and Satheesh, S. K. 2000. Aerosol modulation of atmospheric and surface solar heating over the tropical Indian Ocean. *Tellus* **52B**, 947–958.

Pruppacher, H. R. and Klett, J. D. 1997. *Microphysics of Clouds and Precipitation*, 2nd revised and enlarged edn with an introduction to cloud chemistry and cloud electricity. Kluwer, Dordrecht, 954 pp.

Ramanathan, V., Crutzen, P. J., Kiehl, J. T. and Rosenfeld, D. 2001. Aerosols, climate, and the hydrological cycle. *Science*, **294**, 2119–2124.

Roeckner, E., Siebert, T. and Feichter, J. 1995. Climatic response to anthropogenic sulfate forcing simulated with a general circulation model. In: *Aerosol Forcing of Climate* (eds R. Charlson and J. Heintzenberg). Wiley, New York, 349–362.

Roesch, A., Wild, M., Pinker, R. and Ohmura, A. 2002. Comparison of surface spectral albedos and their impact on the general circulation model estimated surface climate. *J. Geophys. Res.* **107**, D14, doi 10.1029/2001JD000809, ACL 13-1–13–8.

Rossow, W. B. and Schiffer, R. A. 1999. Advances in understanding clouds from ISCCP. *Bull. Am. Meteorol. Soc.* **80**, 2261–2287.

Rossow, W. B., Walker, A. W., Beuschel, D. E. and Roiter, M. D. 1996. *International Satellite Cloud Climatology Project (ISCCP). Documentation of New Cloud Datasets*. World Meteorological Organization, Geneva, 115 pp.

Schwartz, S. E. 1996. The whitehouse effect – shortwave radiative forcing of climate by anthropogenic aerosols. An overview. *J. Aerosol Sci.* **72**, 469–477.

Shaw, G. E., Stamnes, K. and Hu, Y. X. 1993. Arctic haze: perturbation to the radiation field. *Meteorol. Atmos. Phys.* **51**, 227–235.

Schult, I., Feichter, J. and Cooke, W. F. 1997. Effect of black carbon and sulfate aerosols on the global radiation budget. *J. Geophys. Res.* **102**, 30 107–30 117.

Shettle, E. P. and Weinmann, J. A. 1970. The transfer of solar irradiance through inhomogeneous turbid atmospheres evaluated by Eddington's approximation. *J. Atmos. Sci.* **27**, 1048–1055.

Sokolik, I. N. and Toon, O. B. 1996. Direct radiative forcing by anthropogenic airborne mineral aerosol. *Nature* **381**, 681–683.

Stenchikov, G. L., Kirchner, I., Robock, A., Graf, H.-F., Antuna, J. C., Greinger, R. G., Lambert, A. and Thomason, L. 1998. Radiative forcing from the 1991 Mount Pinatubo volcanic eruption. *J. Geophys. Res.* **103**, 13 837–13 857.

Swap, R., Garstang, M., Greco, S., Talbot, R. and Kallberg, P. 1992. Saharan dust in Amazon basin. *Tellus* **44B**, 133–149.

Takemura, T., Okamoto, H., Murayama, Y., Numaguti, A., Higurashi, A. and Nakajima, T. 2000. Global three-dimensional simulation of aerosol optical thickness distribution of various origins. *J. Geophys. Res.* **105**, 17 853–17 873.

Takemura, T., Nakajima, H. T., Dubovik, O., Holben, B. N. and Kinne, S. 2002. Single-scattering albedo and radiative forcing of various aerosol species with a global three-dimensional model. *J. Climate* **15**, 333–352.

Taylor, K. E. and Penner, J. E. 1994. Response of the climate system to atmospheric aerosols and greenhouse gases. *Nature* **369**, 734–737.

Tegen, I., Lacis, A. A. and Fung, I. 1996. The influence on climate forcing of mineral aerosols from disturbed soils. *Nature* **380**, 419–422.

Tegen, I., Hollrigl, P., Chin, M., Fung, I., Jacob, D. and Penner, J. E. 1997. Contribution of different aerosol species to the global aerosol extinction optical thickness: estimates from model results. *J. Geophys. Res.* **102**, 23 895–23 915.

Tegen, I., Koch, D., Lacis, A. A. and Sato, M. 2000. Trends in tropospheric aerosol loads and corresponding impact on direct radiative forcing between 1950 and 1990: a model study. *J. Geophys. Res.* **105**, 26 971–26 989.

Thekaekara, M. P. and Drummond, A. J. 1971. Standard values for the solar constant and its spectral components. *Nature Phys. Sci.* **229**, 6–9.

Torres, O., Barthia, P. K., Herman, J. R., Sinyuk, A., Ginoux, R. and Holben, B. 2002. A long-term record of aerosol optical depth from TOMS observations and comparison to AERONET measurements. *J. Atmos. Sci.* **59**, 398–413.

Twomey, S. 1974. Pollution and planetary albedo. *Atmos. Environ.* **8**, 1251–1256.

Vardavas, I. and Carver, J. H. 1984. Solar and terrestrial parameterizations for radiative convective models. *Planet. Space Sci.* **32**, 1307–1325.

Vitale, V., Tomasi, C., Lupi, A., Cacciari, A. and Marani, S. 2000. Retrieval of columar aerosol size distributions and radiative-forcing evaluations from sun-photometric measurements taken during the CLEARCOLUMN (ACE 2) experiment. *Atmos. Env.* **34**, 5095–5105.

Wild, M, 1999. Discrepancies between model-calculated and observed shortwave atmospheric absorption in areas with high aerosol loadings. *J. Geophys. Res.* **104**, 27 361–27 371.

Zhang, J., Liu, S. M., Lü, C. and Huang, W. W. 1993. Characterizing Asian wind-dust transport to the Northwest Pacific Ocean. Direct measurements of the dust flux for two years. *Tellus* **45B**, 335–345.

Zhang, Y.-C., Rossow, W. B. and Lacis, A. A. 1995. Calculation of surface and top of atmosphere radiative fluxes from physical quantities based on ISCCP data sets, 1. Method and sensitivity to input data uncertainties. *J. Geophys. Res.* **100**, 1149–1165.